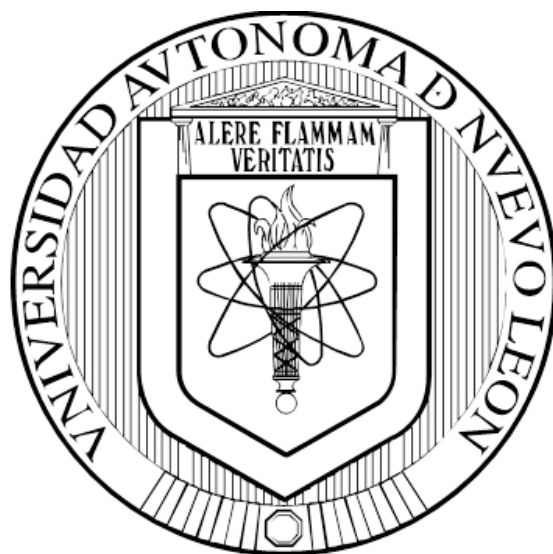


**UNIVERSIDAD AUTÓNOMA DE NUEVO LEÓN
FACULTAD DE CIENCIAS QUÍMICAS**



**FeS₂/ZnO core/shell nanowires: structural, optical and
electrochemical properties**

POR

MARÍA FERNANDA RETANA BETANCOURT

COMO REQUISITO PARCIAL PARA OBTENER EL
GRADO DE MAestrÍA EN CIENCIAS
CON ORIENTACIÓN EN QUÍMICA DE LOS MATERIALES

DICIEMBRE, 2016

Abstract

María Fernanda Retana Betancourt

Graduation date: December, 2016

Universidad Autónoma de Nuevo León, Facultad de Ciencias Químicas

Study Title: FeS₂/ZnO core/shell nanowires: structural, optical and electrochemical properties

Page numbers: 112

Candidate for the degree of Maestro en Ciencias con Orientación en Química de los Materiales

Study Field: Materials science and nanochemistry

Purpose and Study Method: Photovoltaic devices with high efficiencies is a top issue due to the importance of alternative systems for energy generation. Although, many efforts have been done in order to find the characteristics and properties that allow the subsequent production and commercialization, hybrid solar cells represent an interesting option for this purpose. The composition in the photoactive layer is key in order to obtain high values of efficiencies and where the use of nanosized materials with one-dimensional morphology embedded into polymeric matrix allows the improvement of their optoelectronic properties. Thus, it is the aim of this thesis the synthesis of core/shell nanowires and the coupling with a conductive polymer. Materials synthesized in this thesis were FeS₂ (pyrite), ZnO and a polyselenophene. In order to generate one-dimensional materials, AAO templates were used for this purpose and an alternative polymerization method, as aldol condensation was carried out.

Contributions and Conclusions:

ZnO and FeS₂ were obtained by immersion method of AAO templates and by microwave heating method respectively. Optoelectronic properties of ZnO nanotubes were study in order to fill them with FeS₂ (pyrite). FeS₂ (pyrite) was carried out by the study of its mechanism, conditions of temperature, iron and sulfur source, reaction time among others. Core/shell nanowires of FeS₂/ZnO were obtained through AAO template-assisted method and exhibit structural, optoelectronic and morphological properties for its potential application in the photoactive layer of hybrid solar cells. Besides, a polyselenophene was obtained through aldol condensation using non-toxic reagents. The conducting polymer exhibit absorption in visible range and charge transfer due to different interactions.

DIRECTOR'S SIGNATURE: _____

Table of content

Chapter 1

<i>Introduction</i>	1
1.1. World wide energy consumption.....	2
1.2. Solar energy status in Mexico.....	4
1.3. Nanomaterials in solar cells.....	5
1.4. Thesis motivations.....	6

Chapter 2

<i>Concepts and literature review</i>	7
2.1. Nanotechnology.....	8
2.1.2 Fabrication of nanomaterials.....	9
2.2. Semiconductor.....	10
2.2.3. PN-Junction.....	12
2.3. Solar cells and the photovoltaic effect.....	14
2.4. Hybrid solar cells.....	17
2.5. One-dimensional nanomaterials for solar cells.....	21
2.6. Techniques for the synthesis of one-dimensional arrays.....	22
2.7. AAO template assisted synthesis.....	23
2.7.2. Advantages in the synthesis with AAO templates.....	25
2.7.3. Anodization process.....	26
2.8. FeS ₂ (pyrite) as semiconductor.....	27
2.9. Zinc Oxide.....	29
2.10. Conductive polymers and their optoelectronic properties.....	31
2.11. Polyselenophene.....	33
2.12. Literature review.....	35
2.13. Scientific contribution.....	42
2.14. Hypothesis.....	42
2.15. Goals and objectives.....	43

Chapter 3

<i>Materials and Methods</i>	44
3.1. AAO templates fabrication.....	45
3.1.2. Methodology for AAO templates.....	46
3.1.3. Making AAO templates conductive.....	47
3.1.4. Cell design for AAO templates.....	48
3.2. Synthesis of ZnO nanotubes by immersion method.....	49
3.3. Synthesis of FeS ₂ nanowires by microwave heating method.....	50
3.4. Synthesis of 2,5-Selenophenedicarbaldehyde by Vilsmeier-Haack reaction.....	51
3.5. Synthesis of a polyselenophene by aldol condensation.....	53
3.6.2. Ultraviolet-visible spectroscopy (UV-Vis).....	54
3.6.3. Photoluminescence (PL).....	56
3.6.4. Fourier transform infrared spectroscopy (FT-IR).....	57
3.6.5. X-Ray diffraction (XRD).....	58
3.6.6. Scanning Electron Microscopy (SEM).....	59
3.6.7. Transmission Electron Microscopy (TEM).....	60

3.6.8. Cyclic Voltammetry (CV).....	61
3.6.9. Electrochemical Impedance Spectroscopy (EIS).....	63
3.6.9. Differential Thermal Analysis-Thermogravimetric Analysis (DTA-TGA) ..	64
3.6.10. Differential Scanning Calorimetry (DSC)	65
Chapter 4	
Results & Discussions	67
4.1 AAO templates fabrication	68
4.2 ZnO nanotubes	70
4.3. FeS ₂ (pyrite)	72
4.4. FeS ₂ /ZnO	78
4.5. 2,5-Selenophenedicarbaldehyde	80
4.6. Polymerization of 2,5-selenofendicarboxaldehyde.....	86
Chapter 5	
Conclusions.....	88
5.1. Preliminary conclusions.....	89

List of figures

Figure 1. Projection of energy consumption for 2040 (EIA).....	2
Figure 2. Solar irradiance in Mexico.....	5
Figure 3. Scale for nanosized materials.....	8
Figure 4. Scheme for bottom-up and top-down approaches.....	9
Figure 5. Band theory for metals, insulators and semiconductors.....	11
Figure 6. Intrinsic and extrinsic semiconductors.....	12
Figure 7. Formation of a depletion region in a PN-junction.....	13
Figure 8. Generations of solar cells.....	15
Figure 9. Structure of a hybrid solar cell.....	18
Figure 10. Mechanism for HSC.....	19
Figure 11. Structure of AAO and its parameters.....	25
Figure 12. Mechanism of pore formation.....	27
Figure 13. Crystal structure for FeS ₂ (pyrite).....	29
Figure 14. Crystal structures of ZnO.....	30
Figure 15. Conductivity range for conducting polymers.....	33
Figure 16. Structure of selenophene and polyselenophene.....	34
Figure 17. Methodology for the fabrication of AAO templates.....	47
Figure 18. Removal process and Au deposition for AAO templates.....	48
Figure 19. Composition of the cell for the fabrication of templates.....	49
Figure 20. Experimental procedure for ZnO nanotubes.....	50
Figure 21. Experimental procedure for the synthesis of FeS ₂	51
Figure 22. Reaction for the synthesis of 2-selenophenedicarbaldehyde.....	52
Figure 23. Reaction for the synthesis of 2,5-selenophenedicarbaldehyde.....	52
Figure 24. Second reaction for the synthesis of 2,5-selenophenedicarbaldehyde.....	53
Figure 25. Polymerization reaction of 2,5-selenophenedicarbaldehyde.....	53
Figure 26. Electromagnetic spectrum.....	54
Figure 27. SEM micrography, first anodization: 30 min a)X20,000 and b)X100,000.....	69
Figure 28. SEM micrography, first anodization: 2h a)X20,000 and b) X50,000.....	69
Figure 29. SEM micrography, first and second anodization 2h, a) X20, 000 and b) X50,000.....	70
Figure 30. Optical absorption for ZnO nanotubes a) embedded AAO template and ZnO released.....	71
Figure 31. Emission spectra for ZnO nanotubes.....	71
Figure 32. Mechanism for FeS ₂ synthesis.....	72
Figure 33. XRD pattern of FeS ₂	74
Figure 34. Optical absorption of FeS ₂	75
Figure 35. Emission spectra for FeS ₂	76
Figure 36. XRD pattern for FeS ₂ for experiments 1:4 and 1:3.....	77
Figure 37. Emission spectra for FeS ₂ for experiments 1:4 and 1:3.....	77
Figure 38. SEM micrography for FeS ₂ a) ratio 1:4 b) 1:2, c)1:3 and EDS.....	77
Figure 39. UV-Vis spectrum of FeS ₂ /ZnO.....	78
Figure 40. Emission spectrum for FeS ₂ /ZnO.....	79
Figure 41. SEM images for FeS ₂ /ZnO embedded in AAO templates a)X230, b)3.7K and c) 1.2 K and EDS.....	80
Figure 42. FT-IR spectra for monomer obtained.....	81
Figure 43. RMN- ¹ H spectrum for 2-selenophenedicarbaldehyde.....	82
Figure 44. RMN- ¹ H spectrum for A.....	83
Figure 45. RMN- ¹ H spectrum for B.....	83
Figure 46. RMN- ¹ H spectrum for C.....	84
Figure 47. Optical absorption for monomers.....	85
Figure 48. Emission spectra for monomers.....	85
Figure 49. FT-IR spectrum for conducting polymer.....	86
Figure 50. UV-Vis spectra for monomer and polyselenophene.....	87
Figure 51. PL spectrum of a polyselenophene.....	87

List of tables

Table 1. Key criteria for a correct performance of solar cells.	16
Table 2. Properties of one-dimensional nanomaterials.	22
Table 3. Common electrolytes for Al anodization.	24
Table 4. Efficiencies values for solar cells where FeS ₂ (pyrite) was incorporated.	37
Table 5. Parameters evaluated for the synthesis of FeS ₂ (pyrite).	73

List of abbreviations

EIA	Energy Information Administration
PV	Photovoltaic
SENER	Secretaría de Energía
PEMEX	Petróleos Mexicanos
0D	Zero-dimensional
1D	One-dimensional
2D	Two-dimensional
E_g	band gap
1G	First-generation of solar cells
2G	Second-generation of solar cells
3G	Third-generation of solar cells
V_{oc}	Open circuit voltage
HSC	Hybrid Solar Cell
EQE	External Quantum Efficiency
CVD	Chemical Vapor Deposition
D_{int}	Inter-pore distance
D_p	pore diameter
tb	barrier layer thickness
tw	pore wall thickness
UV	Ultraviolet
OLED	Organic Light-Emitting Diode
HOMO	Highest Occupied Molecular Orbital
LUMO	Lowest Unoccupied Molecular Orbital
UV-Vis	Ultraviolet-visible
PL	Photoluminescence
FTIR	Fourier Transform Infrared
DTA-TGA	Differential Thermal Analysis-Thermogravimetric Analysis
FE-SEM	Field Emission Scanning Electron Microscopy
TEM	Transmission Electron Microscopy
CV	Cyclic Voltammetry
EIS	Electrochemical Impedance Spectroscopy
SPR	Surface Plasmonic Resonance
XRD	X-Ray Diffraction
EBSD	Diffraction Backscattered Electron Detectors
CL	Cathodoluminescence
STEM	Scanning Transmission Electron Microscopy

EDS	X-ray Energy-Dispersive Spectroscopy
EELS	Electron Energy-Loss Spectroscopy
SA	Selected Area
NB	Nanobeam
CB	Convergent-Beam
ED	Electron Diffraction
ET	Electron Tomography
E_i	Initial potential
CO₂	carbon dioxide
kWh/m²	kilowatt hour per square meter, unit for energy consumption
nm	nanometers
eV	electron volts
PEDOT	Poly(3,4-ethylenedioxythiophene)
PSS	Polystyrene sulfonate
ITO	Indium Tin Oxide
AAO	Anodic Aluminum Oxide
M	molarity, unit of concentration
V	volt, unit of voltage
FeS₂	Iron disulfide
FeS	Iron sulfide
ZnO	Zinc oxide
Scm⁻¹	siemens, unit of conductivity
CdS	Cadmium sulfide
CdSe	Cadmium selenide
SnS	Tin sulfide
ZnS	Zinc sulfide
CuO	Copper oxide
CuS	Copper sulfide
Cu₂S	Copper(I) sulfide
Bi₂S₃	Bismuth(III) sulfide
FeCl₂	Iron chloride
FeBr₂	Iron bromide
μm	micrometers
PVP	poly(vinyl pyrrolidone)
PEDOS	Poly(3,4-ethylenedioxy-selenophene)
H₂C₂O₄	Oxalic acid

H₂CrO₄	Chromic acid
H₃PO₄	Phosporic acid
CuCl₂	Copper chloride
PVC	Polyvinyl chloride
Zn(O₂CCH₃)₂	Zinc acetate
KOH	Potassium hydroxide
DMF	Dimethylformamide
POCl₃	Phosphoryl chloride
NaOH	Sodium hydroxide
Å	Armstrong, unit of lengths
SCE	Saturated calomel electrode
P3HT	Poly(3-hexyl)thiophene
PCBM	[6,6]-phenyl C61 butyric acid methyl ester

Chapter 1
Introduction

1.1. World wide energy consumption

Everyday high quantities of energy are consumed in order to supply the basic needs for humankind. This energy demand is also increasing as the technology comes forward and there are more human needs. According to the U.S. Energy Information Administration (EIA), the energy demand is projected with an increasing of almost 56% by 2040^[1]. In Figure 1, represents the projection of electricity generation by fuel for 2040.

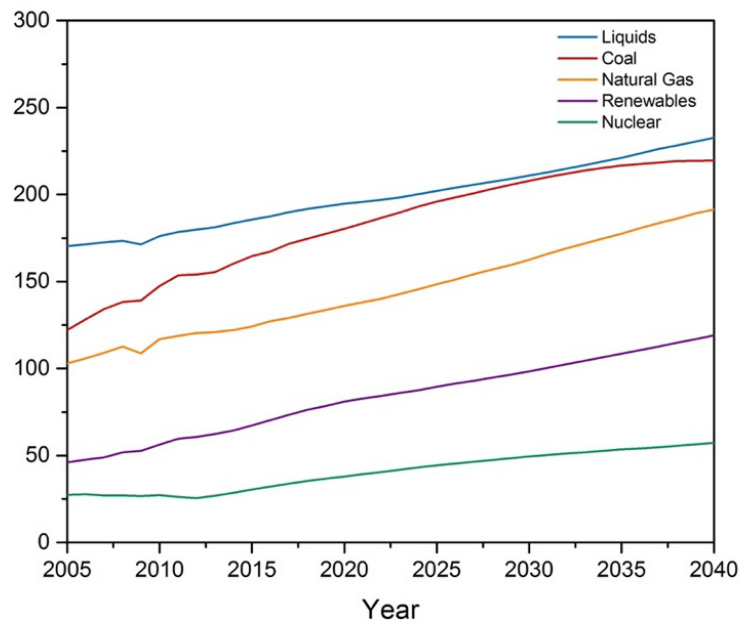


Figure 1. Projection of energy consumption for 2040 (EIA).

Since, it has been demonstrated energy demand is related with environmental impact, 80% of energy come from fossil fuels producing high concentrations of CO₂, the development of systems that contributes with cleaner and more efficiency energy represents a top field of study.

The use of this alternatives resources will produce not only the reduction of greenhouse effects but also, the diversification of energy supplies, stimulate the creation of new jobs, create competitiveness between energy suppliers and reduce the fossil fuels dependence.

Some of the alternative and renewable resources are:

- **Biomass energy:** the energy comes from living or recently living organisms, since organic matter can store energy due to the photosynthesis process.
- **Geothermal energy:** corresponds to thermal energy from inside the Earth.
- **Wind energy:** describes the process by which the wind converts kinetic energy into mechanical energy through wind turbines.
- **Hydroelectric energy:** the production of energy due to the gravitational force of falling or flowing water.
- **Solar energy:** energy comes from the sun through a photovoltaic (PV) module by which converts solar energy into electrical energy.

The reasons of why solar energy is considered one of the key solution for energy demand is due to solar energy reaches the surface of earth at rate of 120 petawatts, it means the energy received can satisfied the increasing energy demand ^[2]. Also, it is a clean and renewable resource with minimal impact in the environment.

1.2. Solar energy status in Mexico

In Mexico, almost the 90% of energy came from fossil fuels according *Secretaría de Energía* (SENER) in 2011 and around 21% came from renewable resources mostly from wind power ^[3]. Although, in recent years has been promoted the use of this clean resources due to the oil reserves are estimated that only last 32.9 years according to PEMEX ^[4].

In 2014, “Energetic Reform” establishes actions in order to solve the actual energetic situation through:

- a) **Energy security:** enough and good quality of energy for the population.
- b) **Economic and production efficiency:** efficiency and competitive prices in the development of energy.
- c) **Environmental sustentability:** low-impact at the environment due to the consumption and development of energy ^[5].

“Energetic Reform” also covers, the exploitation of alternative resources in order to supply clean and sustainable energy. Among the renewable resources, the sun power in Mexico represents an attractive opportunity for the generation of electricity through photovoltaics systems since the country belongs to the “sunbelt” with a average irradiance between 5 kWh/m² per day and 6 kWh/m² per day as can be seen in Figure 2 ^[6]. Thus, Mexico is a potential country for the investment in photovoltaic modules and energy power generation, only behind of China and Singapore ^[7].

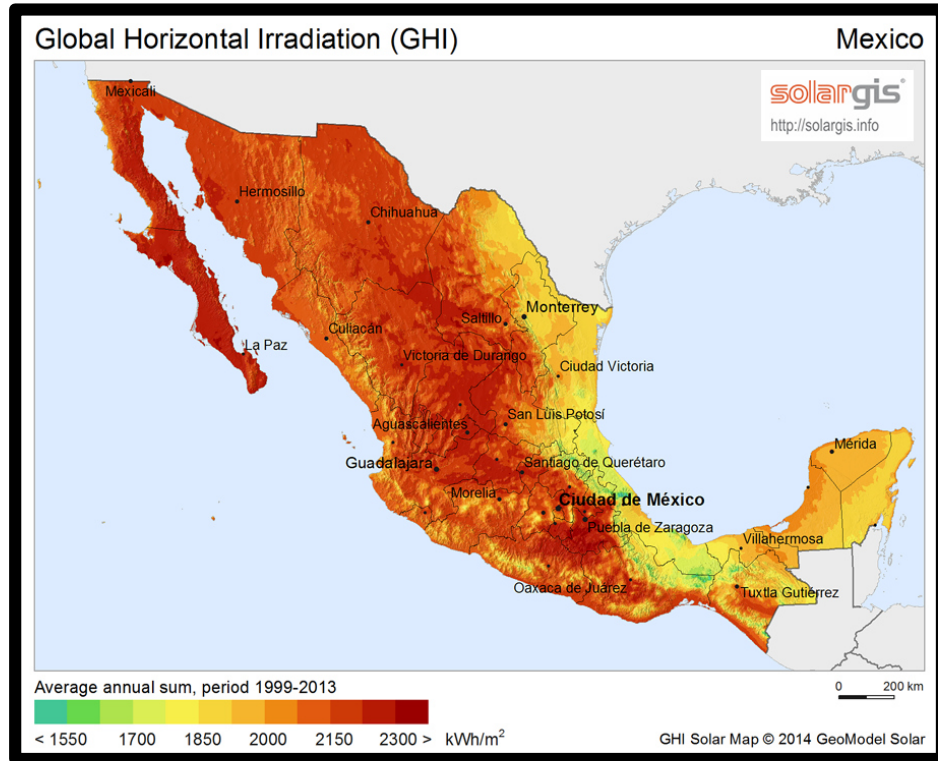


Figure 2. Solar irradiance in Mexico.

1.3. Nanomaterials in solar cells

Nanomaterials play an interesting role in different fields because of their characteristics dimensions, physical properties, chemical stability, size, morphology etc. Due to all and more properties nanomaterials represents an advantage for energy conversion and storage. One of the goals in solar cells are the enhancement of their optical properties and here the nanomaterials offer the possibility of improving the absorption in the active layer or reducing the exciton recombination. Also, nanomaterials can exhibit multiple exciton generation, large surface area and improving electron transport trough the use of one-dimensional nanostructures [8].

Through, nanochemistry semiconductor quantum confined nanomaterials, sensitizing dyes and polymers can be incorporated into one and unique system improving exciton separation, charge transport and collection. The use of hybrid systems leads the presence of phenomena as multi-exciton generation, singlet exciton fission, plasmonic-induced light trapping, as well as photon up-conversion and down-conversion breaking the Shockley–Queisser limit set for a single junction solar device ^[9].

High efficiencies of photovoltaic modules and keeping manufacture cost low is the main target for an increasing demand of this electrical power generators where nanomaterials and nanotechnology play a key role.

1.4. Thesis motivations

Bearing in mind the importance of nanosized materials embedded into polymeric matrix in order to improve their optoelectronic properties for their use in hybrid solar cells, it is the aim of this thesis the synthesis of one-dimensional nanostructures and the coupling with a conductive polymer.

Chapter 2

Concepts and literature review

This chapter contains the basics concepts and framework for a complete understanding of the topics involved in this thesis. This chapter includes information about hybrid solar cells, the semiconductors characteristics and conductive polymers for their use in photovoltaic systems.

2.1. Nanotechnology

In 1959, the idea of manipulation at atomic level was described by the physicist Richard Feynman and currently, represents the most versatile and powerful tool for the fabrication of better devices that satisfy human needs. The nanoscience studies the properties of materials at nanoscale while, nanotechnology describes the manipulation, research and creation of devices at atomic and molecule level. Nanoscale is considered in the range of 0.1- 100 nm^[10-11]. In Figure 3 shows schematically the nano size.

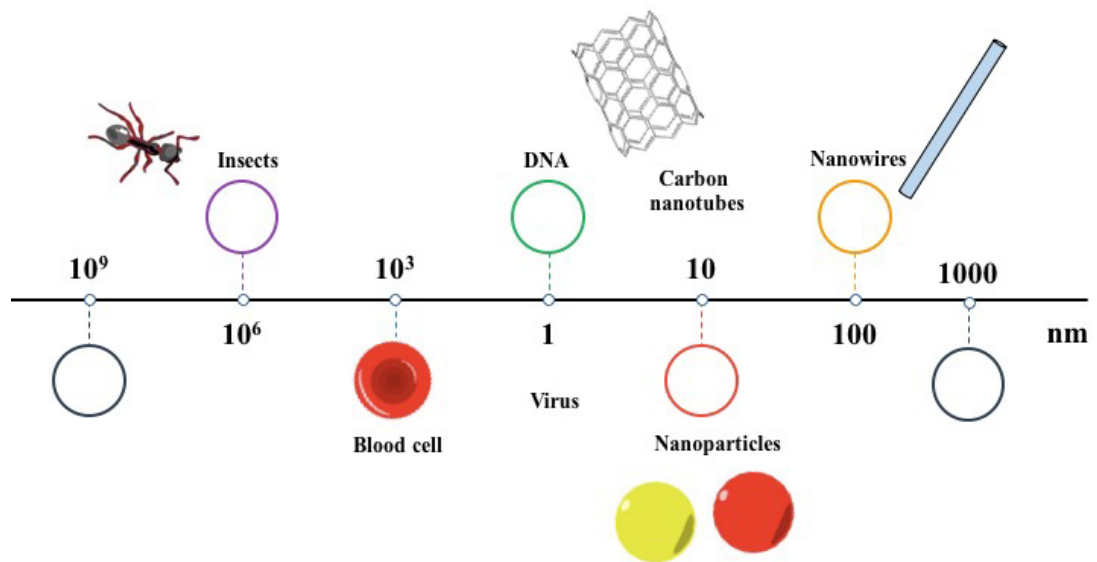


Figure 3. Scale for nanosized materials.

The development of nanotechnology bring us knowledge, innovation and new technology. It is important to remark since the application of nanotechnology has been a boom in the development of technology which is not odd to find everywhere e.g. TV's, smartphones, laptops, beauty supplies, energy storage among others.

2.1.2 Fabrication of nanomaterials

For the obtaining of nanomaterials is categorized in two class of process:

- a) **Top-down:** refers to cut, mill or slice continuously a bulk material until nano sized particle. Lithography, nanolithography, milling are the common approaches for top-down methods.
- b) **Bottom-up:** refers to the construction of structures atom by atom, molecule by molecule or cluster by cluster. The common techniques are chemical synthesis, self-assembly and deposition ^[11-12].

Figure 4 illustrates the bottom-up and top-down approaches.

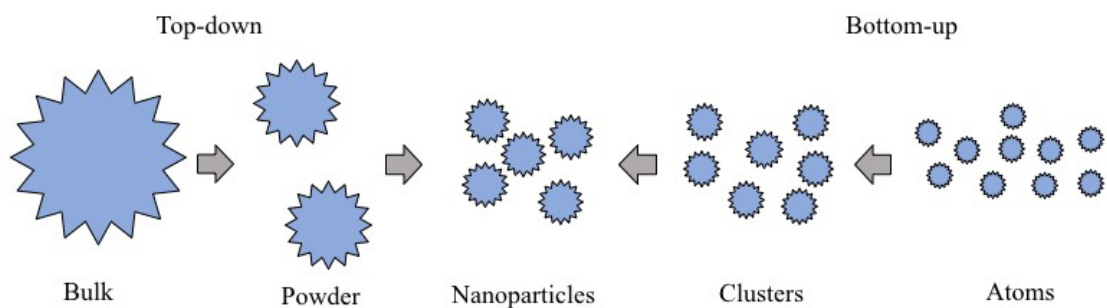


Figure 4. Scheme for bottom-up and top-down approaches.



The obtained nanomaterials are usually classified as inorganic or organic materials but they are also classified based on their dimensionality: Zero-dimensional (0D) as quantum dots and metal nanoparticles. One-dimensional (1D) as nanowires, nanorods and nanotubes and two-dimensional (2D) as thin films, surfaces and interfaces ^[13].

Nanotechnology have a number of papers of several nanomaterials in distinct morphologies and sizes and in different fields as medical, food industry, pharmaceutical industry, space industry, energy conversion and storage among others. The last one is the main application of this thesis and will be described extensively in the subsequent sections since nanotechnology provides an enormous field of opportunities and contributions for energy conversion and storage.

2.2. Semiconductor

Semiconductors are the essential part of a photovoltaic solar cell and their basic characteristics are described in this section.

Every solid contains electrons. In crystals, electrons are arranged in energy bands separated by regions in energy for which no wavelike electron orbital exists. These forbidden regions are called energy gaps or band gaps (E_g), and result from the interaction of conduction electrons waves with the ion cores of the crystal ^[14].

Figure 5 shows the scheme for metals, semiconductors and insulators according to the band theory where the energy gap for metal doesn't exist between filled and unfilled



energy levels. Several electrons are thermally excited into empty levels, creating holes in the filled band. For semiconductors, band structure is divided in: conduction band and valence band. This one is full filled of electrons while conduction band is unfilled of electrons. In semiconductors E_g is small, but large enough so that a fairly small number of electrons are in the conduction band due to stimuli of pressure, temperature or irradiation influence ^[15]. In insulators E_g is large so that electrons are not promoted to the conduction band due to thermal energy, and these materials do not conduct electricity.

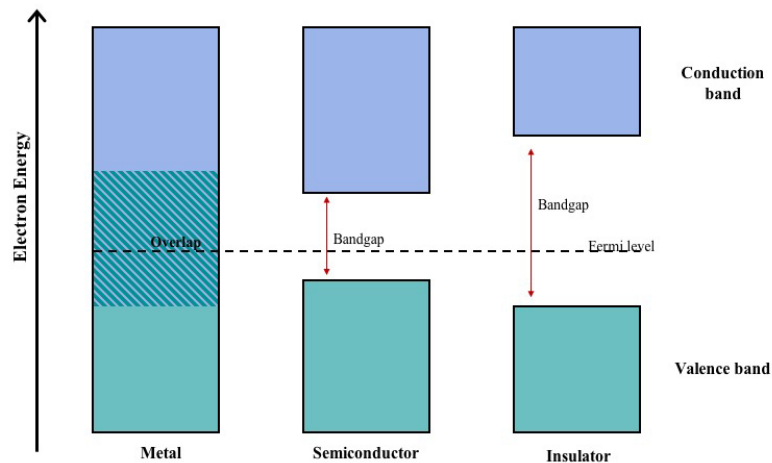


Figure 5. Band theory for metals, insulators and semiconductors.

2.2.2. Classification of semiconductors

Semiconductors can be classified into the following type ^[16-18] and are illustrated in Figure 6:

- a) **Intrinsic type (element)** also known as pure or undoped semiconductors, describe perfect semiconductor crystals which are free from defects and impurities of other elements.

b) **Extrinsic type (compound or alloys)** corresponds to the inclusion of foreign atoms in the crystal lattice, this phenomena es called doped and can be in two ways:

- i. **n-type:** referes to the donation of an excess of electrons in the host lattice, the incorporated atoms are denoted as “donors”.
- ii. **p-type:** occurs when there is a missing electron in the host lattice and at the same time a hole appears near the upper edge of the valence band of the latter. The incorporated atoms are called as “acceptors”.

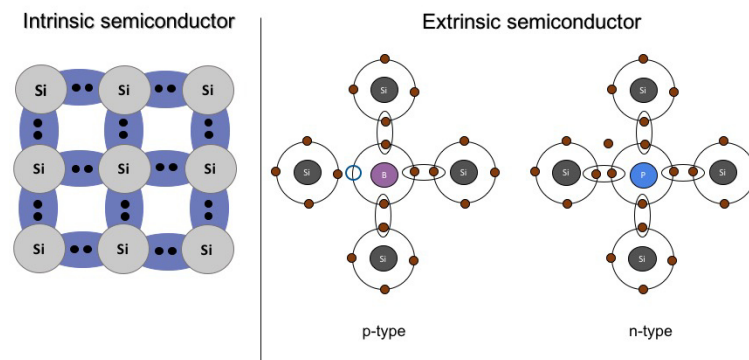


Figure 6. Intrinsic and extrinsic semiconductors.

2.2.3. PN-Junction

A PN-junction consists in the joining p-type semiconductor material with n-type semiconductor. Even when both sides are electrically neutral, diffusion current occurs due to the high concentration of electrons and holes, free electrons move across PN-junction from n-type to p-type. Diffusion would continue until free electrons and holes are distributed in both materials. However, an electric field in both sides are established due to diffusion. It is negative on the p-type material and positive on the n-type semiconductor due to the loss of free electrons. This electrical field prevents further diffusion as the

electrons on the n-type side are expelled from the p-type side by the electrical field. Figure 7, represents PN-junction and the corresponding diffusion process.

The effects of both diffusion and electric field eventually lead to an equilibrium where no free charge carriers can rest in a position where there is a potential barrier. This region around the PN-junction, called the depletion region as there no longer exist freely movable charge carriers, becomes a barrier between the two ends of the material that prevent current to flow through. The total charge on each side of a PN Junction must be equal and opposite to maintain a neutral charge condition around the junction. If the depletion layer region has a distance D , it therefore must therefore penetrate into the silicon by a distance of D_p for the positive side, and a distance of D_n for the negative side giving a relationship between the two of $D_p \cdot N_A = D_n \cdot N_D$ in order to maintain charge neutrality also called equilibrium. Figure 7, shows the formation of depletion region and distance between n-type and p-type semiconductor ^[19].

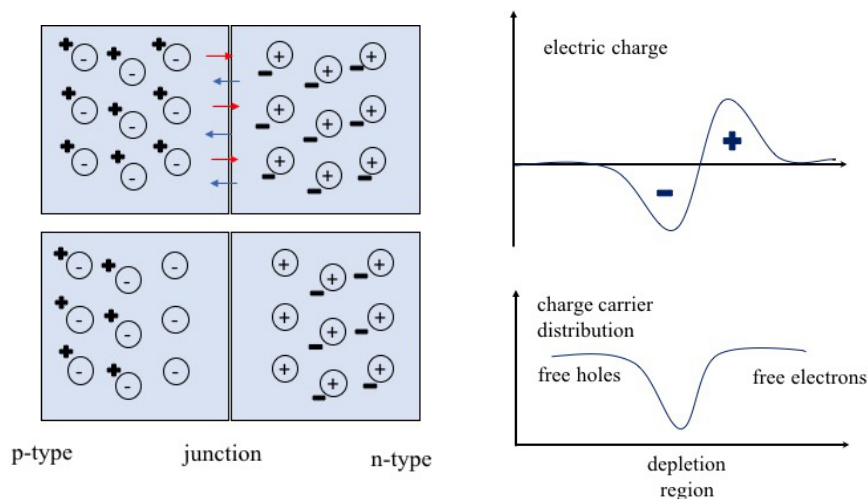


Figure 7. Formation of a depletion region in a PN-junction.

2.3. Solar cells and the photovoltaic effect

At this stage, clean and eco-friendly sources of energy are considered part of the solution for the increasing energy demand where solar energy plays an important role due to is an abundant and renewable resource.

Through the years, the study of solar energy conversion is a field with many reports where the search for low-cost, high efficiencies and eco-friendly systems is still being studied. At this stage three generations have been purposed, first-generation (1G) of solar cells included crystalline and polycrystalline silicon based modules which currently, dominate the market, their power efficiencies are in the range of 21 to 25 %^[20]. Although, the high-cost of manufacturing, installation and availability of Si concerns about if this material can provide enough photovoltaic modules for the increasing energy demand.

In order to produce low-cost modules with high efficiencies, second-generation (2G) thin solar films and amorphous silicon solar cells were released, their principal advantage is their flexibility allowing modules could be on the roof tops. Third-generation (3G) represents the most versatile stage due the different materials which are used in the modules. Polymer-based, dye-sensitized or nanostructured solar cells are some of the innovative alternatives^[21-22]. Also, this generation try to provide low-cost and high efficiency devices. Figure 8, represents the three generations of solar cells.

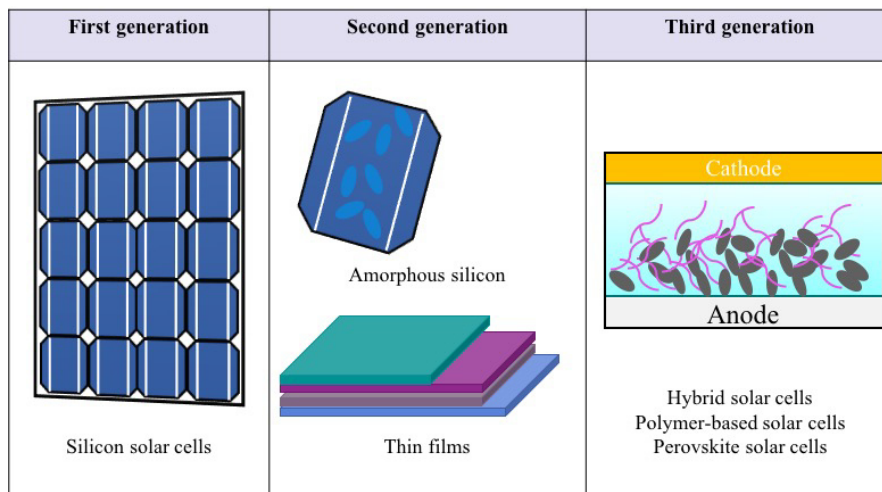


Figure 8. Generations of solar cells.

As can be noticed many efforts have done in order to provide photovoltaic solar cells with desirable characteristics as high efficiency, low-cost and eco-friendly modules. Since the fabrication of thin films or nanocrystals for the PV application is not an easy task different criteria influence the performance of a solar cell, Table 1 summarizes the characteristics ^[23].

Inorganic and organic semiconductors have been purposed in several papers in the pursue of a solar cell that accomplish all the characteristics (Table 1), but even high contribution has made in this field, solar cells with efficiencies higher than 20% have not been fabricated thus, solar cells researchers agree that nanomaterials, the combination of different inorganic semiconductors (e.g. core/shell nanostructures, decorated inorganic systems) and the incorporation of conductive polymers can be the key for photovoltaic modules capable to transform solar energy into electrical with better efficiency, with long-

life time of the solar cell and also, an important factor with low-cost and abundant materials.

Table 1. Key criteria for a correct performance of solar cells.

Property	Criteria
Band gap of smaller band-gap materials	Eg near 1.4 eV to maximize absorption of solar radiation, while minimizing diode current that limits V_{oc} . Direct optical absorption so that carriers are generated close to the junction. Long minority-carrier diffusion length
Larger band-gap material	As large as possible while maintaining low series resistance
Conductivity type	Smaller band gap materials should usually be p-type because of longer electron diffusion lengths
Electron affinities	Materials should be chosen such that no potential spike occurs at the junction for the minority photoexcited carriers
Diffusion voltage	As large as possible, since the maximum V_{oc} is proportional to the diffusion voltage
Lattice mismatch	As little mismatch in lattice constant between the two materials as possible (this appears to minimize interface state density and recombination losses through such states)
Deposition methods	Suitable deposition methods for thin-film formation and control should be available
Electrical contacts	It should be possible to form low-resistance electrical contacts to both n- and p-type materials
Materials availability	Supplies of the materials should be sufficient to allow large-area cell production
Material cost	Cost of the material should be competitive with alternative systems
Material toxicity	Material should be non-toxic, or control of toxicity should be possible
Cell stability and lifetime	Cell must have an operating lifetime sufficient to pay back economic and energy costs required to produce it

In order to understand how the previous characteristics domain, the correct performance of a solar cell is important to describe that the physics in solar cells is based in the PV effect. The photovoltaic effect is the process where electrical potential is generated by materials when they are exposed to a source of electromagnetic energy. The intensity of the photovoltaic effect is strongly correlated to the intensity of the light source, the constituent wavelengths of the supplied light and the physical makeup and structure of the incident material. It has been found that the greatest power output available from the photovoltaic effect, if using sunlight as your electromagnetic power source, can be generated using either silicon or another semiconductor material ^[24].

In the next section it is described how hybrid solar cells work since each configuration and combination of materials impact in a different way into the electrical conversion.

2.4. Hybrid solar cells

Hybrid solar cells (HSC) emerged as an alternative solution for energy demand since Si modules cost and availability represents a disadvantage for their future commercial process. HSC mix both inorganic and organic materials in order to combine their unique optical, structural and electrical properties. In a general way, HSC involves the use of inorganic nanoparticles (a semiconductor type “n”) and a conducting polymer (a semiconductor type “p”) ^[25-26].

Organic conductive semiconductor have interesting properties for photovoltaics systems due to their easy processing, possible recyclability, relatively low cost, scalability and applicability as sustainable materials. While inorganic semiconductor possesses better electronic properties, e.g. a high dielectric constant, a high charge mobility and thermal stability etc., their nanoparticles exhibit enhanced electronic, photoconducting and luminescent properties ^[27]. All these advantages combine in a unique system make HSC an interesting and promising candidate for electrical generation.

The basic structure of a HSC consists at least of four layers which are cathode, a metal of low work function (Al, Ag, Au, etc.) that allows the electrons transports between conduction band and metal. The hole transport layer, usually PEDOT:PSS due to its transparency, mechanical flexibility and thermal stability. Active layer, the principal layer in HSC since here occurs the absorption of light, diffusion and recombination of excitons and charge carrier diffusion. The anode also consists of a conductive metal. The last important part of the solar cell is the substrate and the suitable substrate for this kind of solar cell is ITO (Indium Tin Oxide) for its conducting properties and transparency that allows light passes through until active layer ^[28]. Figure 9, illustrates the structure of HSC.

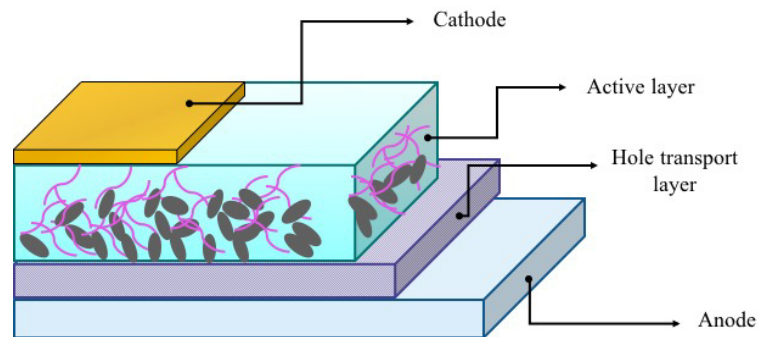


Figure 9 Structure of a hybrid solar cell.

One step key for a better efficiency of HSC is the interfacial charge separation in the active layer. Distinct parameters govern the charge separation that occurs in this interface, some of them are interface area, the nominal interfacial driving energy, the morphology of the interfaces/domains, the interfacial layer/molecules/bridges, the crystallinity of the components, the mixture homogeneity, and the migration of separated charges from the interfaces. The effect of those factors increase or decrease the photovoltaic conversion efficiency ^[29].

The importance of the interface is due to here occurs the whole process of light absorption, the electron-hole pairs are generated subsequently, exciton diffuse into a donor-acceptor interface in order to dissociate in free charges. Then, electrons migrate to electrodes and finally are collected by them ^[30]. The mechanism of the charge separation process is illustrated in Figure 10 and explained in 6 key steps:

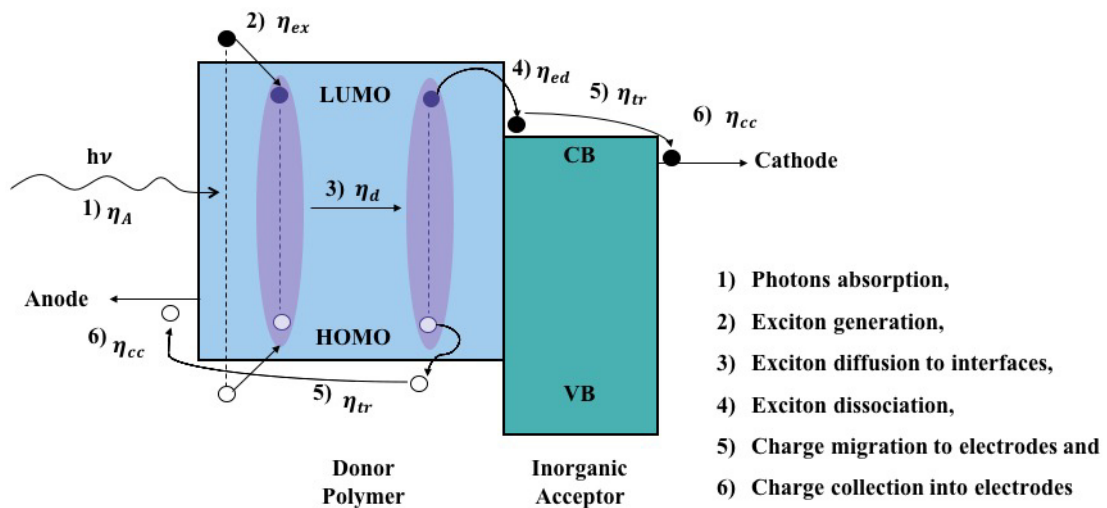


Figure 10. Mechanism for HSC.

The six steps determine the external quantum efficiency (EQE) which is a percentage of the number of charge carrier collected at the electrode to the number of photons incident on the device. It can be expressed by the equation 1^[30-31]:

$$EQE = \eta_a \times \eta_{ex} \times \eta_{diff} \times \eta_{ed} \times \eta_{tr} \times \eta_{cc} \quad \text{Eq. (1)}$$

Since the donor-acceptor interface is crucial for a better performance of the solar cell, the architecture plays an important role. Different configurations of hybrid solar cells can be fabricated.

- a) **Planar bilayer:** coatings of distinctive film of conductive polymer on inorganic semiconductor layer.

- b) **Bulk heterojunction:** conductive polymer and inorganic semiconductor are blending during the synthesis and later, deposited on a substrate. The principal advantage of this architecture is the low cost allowing their commercial development and the exciton dissociation shows an improvement compared to bilayer solar cells.

- c) **Ordered heterojunction layer:** since high efficiencies are important for the operation, ordered heterojunction are fabricated infiltrating nanomaterials during or after polymerization. Although, the carrier transportation and surface area shows

an enhancement, this configuration is not the most popular due to the cost-effectiveness and methods to synthesize ordered nanocomposites^[32].

Since the thickness is a crucial parameter for thin films different values of thickness have been reported although most of the papers agree that the thickness between 100-300 nm is enough to absorb light. It could be thought a thicker active layer would absorb more light although, the charge transport and collection will be negatively affected^[33].

Parameters as the molecular weight of conductive polymer and inorganic semiconductor morphology have an important role in solar cell performance and will be discussed in the following sections.

2.5. One-dimensional nanomaterials for solar cells

One-dimensional (1D) nanomaterials are promising candidates to improve the performance for solar cells due to their anisotropic properties and also, for the characteristics describe in Table 2^[34]:

The most-common morphologies for 1D nanomaterials includes nanorods, nanobelts, nanotubes, nanofibers, nanopillars, nanowires and so on. Generic methodologies to synthesize 1D nanomaterials are limited. Thus, the following section details the methodologies used to obtain inorganic 1D nanostructures.

Table 2. Properties of one-dimensional nanomaterials.

Property	Contribution
Transparency and conductivity	1D materials provide enough interspace among them for the penetration of incident light, which can strike an excellent balance between the transparency and conductivity.
Surface area	larger specific areas enable sufficient charge generation, separation, and collection, which lead to higher device performance.
Charge transport	1D materials provide a direct charge transport and decreases electrical resistance compared to nanoparticles.
Oriented structure	improve the mechanical and electrical properties of nano- materials on the oriented direction, and are favorable for improving device performance.

2.6. Techniques for the synthesis of one-dimensional arrays

Several techniques have been reported for the synthesis of 1D nanostructures as chemical vapor deposition (CVD), sol-gel, hydrothermal, electrodeposition etc., but the main problem is the high polydispersity of these systems. Some variations in these techniques has been made and good results have been obtained although, the problem is the high cost for the specialize equipment ^[35]. An attractive alternative is the use of templates since it can be obtained materials with low-dispersity due to the dimensional control, they permit the designing of nanomaterials with desirables characteristics according the final application and also, this technique is highly reproducible ^[36]. The synthesis of templates requires of the anodizing process where, the metal is oxide producing an anodic oxide layer. Several anodic oxide layers in different materials have been studied for example, Mg, Zn, Sn, Zr, Al among others ^[37].

As mentioned, the anodization process for Al metal produces anodic aluminum oxide (AAO) and it has become a key technique for the synthesis of one-dimensional materials due to its controllable characteristics of shape and dimensions of pore, periodicity and high distribution ^[38]. Template-assisted electrodeposition is a flexible method for the synthesis of 1D semiconductor nanostructures. Growth can be controlled when a current or potential is applied then cations and anions diffuse towards the bottom of the pore where electrochemical reactions take place until the material is obtained. Diameter and length of 1D can be tuned by AAO pore size and by the time of electrodeposition respectively. However, maximum length of these 1D nanostructures is limited by the thickness of the template membrane (50–60 μm for commercial alumina). Diameters can range from 10 nm to 1 μm ^[39-41].

2.7. AAO template assisted synthesis

Al metal is an important element for several industrial applications i.e. aerospace, building, sports, packaging, transportation, etc., and represents a little over the the 8% of Earth's crust ^[42].

Since the anodization process an anodic oxide layer is formed, it is important to remark the mechanism that occurs during this process since the understanding of this process permits a correct designing of parameters in order to obtain nanomaterials with desirable characteristics.

Firstly, the oxide layer consists in two distinct layers, the barrier layer which, it is a non-porous thin layer and depends substantially of the nature of electrolyte (concentration, pH) since electrolyte commonly is an acid. Different acids have been studied but the more common acids are oxalic acid, phosphoric acid and sulfuric acid. The second layer consists of a hydrated porous layer growing on top of the barrier layer^[43-44]. Table 3 enlisted some of the acidic media used for Al anodization.

Table 3. Common electrolytes for Al anodization.

Electrolyte	Concentration (M)	Voltage (V)	Pore diameter (nm)	Reference
Sulphuric acid (H ₂ SO ₄)	0.18-2.5	15-25	15-25	[45-46]
Phosphoric acid (H ₃ PO ₄)	0.04-1.1	100-195	130-250	[45,47]
Oxalic acid (H ₂ C ₂ O ₄)	0.2-0.5	30-80	40-100	[45,48]

Figure 11, shows the structure of AAO prepared by electrochemical anodization. The structure of AAO can be described as a close-packed hexagonal array of parallel cylindrical nanopores perpendicular to the surface on top of the underlying Al substrates. The structure of self-ordered AAO is often defined parameters such as: interpore distance (D_{int}), pore diameter (D_p), barrier layer thickness (t_b), pore wall thickness (t_w), pore density (ρ) and porosity (P). These parameters can vary in the range of about 50-60 nm for D_{int} , 10-400 nm for pore diameter, a thickness of the porous layer from 10 nm to 150 μm , a pore aspect ratio from 10 to 5000 a pore density from 10^9 to 10^{11} cm^2 and porosity from 5 to 50%^[40,49].

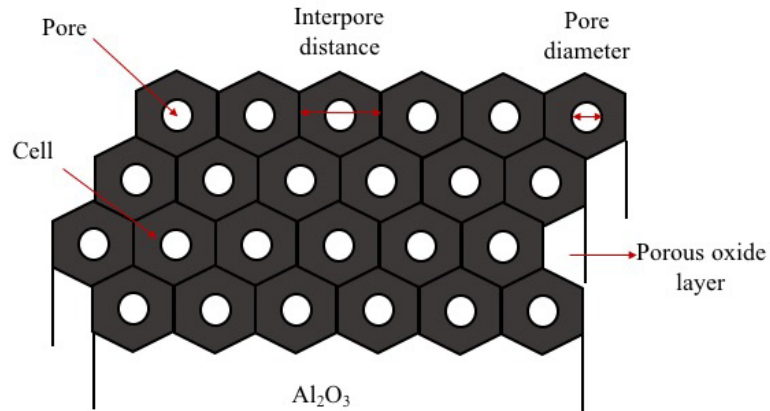


Figure 11. Structure of AAO and its parameters.

2.7.2. Advantages in the synthesis with AAO templates

As mentioned in section 2.6, different techniques have been reported for the synthesis of one-dimensional nanomaterials but one desirable characteristic is the vertical alignment of the material. The use of AAO templates not only have this advantage but also, the following:

- Pore sizes can be controlled permitting nanomaterials with controlled diameters.
- Aligned growth, perpendicular to substrate.
- Different kind of materials can be deposited: oxides, metals and polymers. Also, distinct morphologies as nanowires, nanorods and nanotubes.
- Control on the dimensions, geometries and formation parameters^[50].

2.7.3. Anodization process

Matsuda *et al.* in reported for the first time the two-step anodization since previous works has been carried out for the Al anodization with only one-step anodization with poorly results ^[51]. The implementation of a second-step allows the formation of a porous oxide layer.

In a general way the anodization process for Al can be divided in:

- **Pre-treatment**, in order to remove scratches, defects and oxides.
- **First-anodization**, here the oxide layer growths.
- **Second-anodization**, during this process occurs the nucleation ^[52].

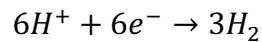
An exact mechanism of pore nucleation is still unknown. However, distinct models try to explain such pore formation. Figure 12 shows the pore formation mechanism in an acidic electrolyte where in the first stage of the anodization Al^{3+} ions migrates from the metal/oxide interface into the forming oxide layer. Meanwhile O^{2-} ions from water travel into oxide layer. During this step ions Al^{3+} and O^{2-} contributes to barrier layer formation, the remaining Al^{3+} ions are dissolved into the electrolyte. This condition is necessary for porous oxide growth, in which Al-O bonds in the oxide lattice break to release Al^{3+} ions. During the oxide formation the barrier layer constantly regenerates with further oxide growth and transforms into a semi-spherical oxide layer of constant thickness that forms the pore bottom ^[53-54].

Reactions for the steps of anodization are the following:

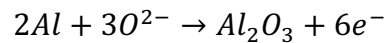
- Al dissolution:



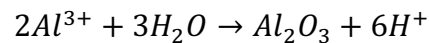
- The production of hydrogen gas at the cathode:



- In the anode takes place reactions at metal/oxide interface



- At oxide/electrolyte boundary:



- Overall anodization of Al equation:

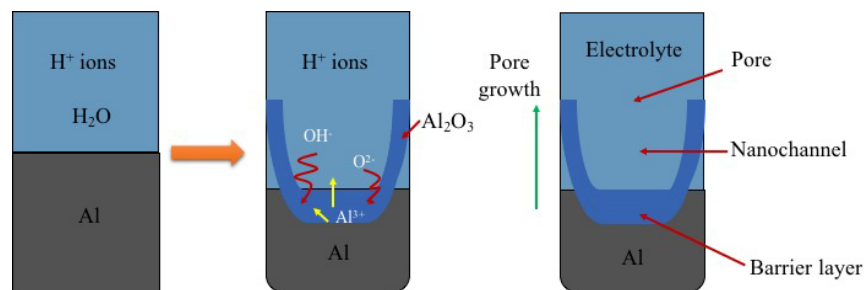
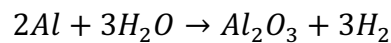


Figure 12. Mechanism of pore formation.

2.8. FeS₂ (pyrite) as semiconductor

Trough the years, researchers have focused in the development of different semiconductors at micro and nanoscale, controlling their morphology and size in order to provide adequated materials capable to convert efficiently solar energy into electrical.

A number of papers have been published with distinct semiconductors incorporated in different kind of solar cells.

Lately, the synthesis of semiconductor have focused in the synthesis of low-cost materials in order to be affordable the mass production of solar cells. Wadia *et al.* in 2009, reported the evaluation of 23 semiconductors with potential properties for photovoltaics technologies. In a general way, FeS₂ by itself represents the cheaper option but also, a high annual electricity production potential. ^[55].

Commonly, FeS₂ (pyrite) is known as fool's gold and is found in the earth's crust in 5 %. It owns a large optical absorption ($\alpha > 10^5 \text{ cm}^{-1}$), a Shockley-Queisser limit around 31%, efficient carrier extraction, non-toxicity, suitable band gap (0.95 eV) and charge mobility of $360 \text{ cm}^2 \text{ V}^{-1} \text{ s}^{-1}$ ^[56-60].

Pyrite structure corresponds to the cubic system (space group $P\bar{a}3$). The Fe atoms are octahedrally coordinated to six sulfur atoms and are at the corners and face centers of the cubic unit cell, while the sulfur atoms are tetrahedrally coordinated to three iron atoms and one sulfur atom. The axes of the S₂ dumb-bells are aligned along the four equivalent $\langle 111 \rangle$ directions ^[61]. In Figure 13, can be seen the corresponding structure for FeS₂.

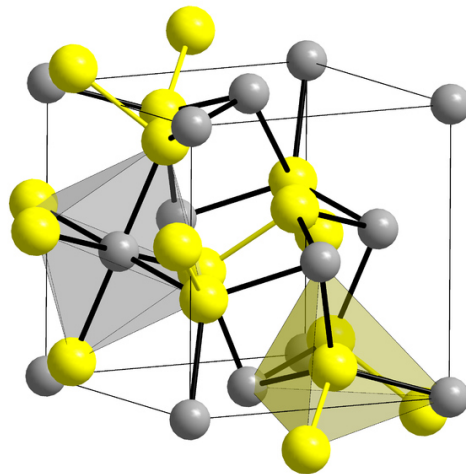


Figure 13. Crystal structure for FeS₂ (pyrite)

It is well known that during the synthesis of FeS₂ appeared impurities as troilite (FeS), greigite (Fe₃S₄), marcasite (FeS₂), pyrrhotite (Fe_{1-x}S) among others ^[62], which are responsible of the poor efficiencies in solar cells and are part of challenge of the synthesis of this promising candidate for photovoltaics technologies.

2.9. Zinc Oxide

A variety of nanostructures and sizes have been developed for ZnO due to its promising properties for an amount of applications among them electronic, optoelectronic, electrochemical, and electromechanical devices, such as ultraviolet (UV) sensors , light-emitting diodes, field emission devices, solar cells and piezoelectric nanogenerators.

ZnO in its mineral way is known as zincite. It corresponds to a semiconductor type “n”^[63]. It owns different crystal structure as wurtzite, zinc blende, and rock salt^[64]. Figure 14, represents its crystal structure being wurtzite the most stable thermodynamically.

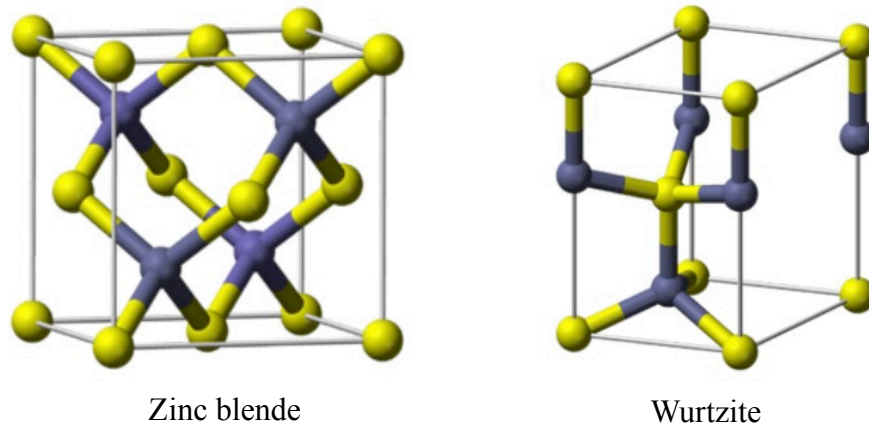


Figure 14. Crystal structures of ZnO.

The wurtzite structure is a hexagonal close-packed structure, where each zinc atom is surrounded by a tetrahedron of four oxygen atoms and vice versa, thus forming an alternate combination of planes of oxygen and zinc atoms, respectively. All tetrahedra are oriented in one direction, and their stacking produces the ZnO hexagonal symmetry^[65].

As properties, ZnO exhibits a band gap of 3.37 eV, non-toxicity, low-cost, is easy to obtain, high stability, charge mobility of $115\text{--}155\text{ cm}^2\text{ V}^{-1}\text{ s}^{-1}$, high thermal conductivity, UV absorption in the range 200–350 nm and emission in the near UV and visible range from 500 to 600 nm and piezoelectricity^[66-68].

Also, the possibility of obtaining different nanostructures of ZnO as 0D (i.e., nanoclusters and nanoparticles), 1D (i.e., nanotube, nanowires, nanorods, and nanobelts), 2D (i.e., nanoplates and layers), and 3D (i.e., nanotetrapods, nanoflowers), have made of it one of the most versatile semiconductors ^[69].

2.10. Conductive polymers and their optoelectronic properties

Commonly, polymers are known for their insulator properties although since the discover of conducting (polymer of Shirakawa) by Shirakawa *et al.* and awarded in 2000 with a Nobel prize, a brand new class of polymers started to be studied ^[70]. This discover resulted in new material which can be implemented in different devices as the organic light-emitting diode (OLED), solar cells, sensors, electronic devices etc., due to their numerous characteristics.

Special characteristics are needed in order to the polymers exhibit conducting properties. Conducting polymers can be defined as a system with semicrystalline zones alternated with large domains of amorphous material ^[71], their chemical structure corresponds to an alternating single bond-double bond (conjugation) along the backbone with sp^2 hybridized in π -bonding and orbitals of carbon atoms which are overlaped causing a system with highly delocalized π -electron and large electronic polarizability ^[72-73]. However, their high polarizability is due to isomeric effect while, electrons in the p_z orbitals of each sp^2 -hybridized carbon atoms form collectively the π band of the conjugated polymer.

π - π^* transitions between bonding and antibonding p_z orbitals allows the absorption within visible light absorption and electrical charge but also, polarizability and π -electron delocalized results in the low ionization potential, low energy optical transitions and high electron affinity which, also depend of defects as solitons, polarons and bipolarons ^[74].

The presence of extensive conjugation in these materials reduces the band gap between the HOMO/valence and LUMO/conduction bands, essentially making them small band gap semiconductors. However, band gap reduction due to the conjugation is not sufficient to achieve appreciable electrical conductivities and the conjugated polymers in their undoped state are semiconductors or insulators. High values of conductivity are usually obtained in doped polymers where dopants alter the band structure of the semiconducting polymer backbone, resulting in the formation of charge carriers such as electrons or holes due to the type of dopant. Usually, conducting polymers are oxidized during the synthesis in order to neutralized is necessary adding a dopant which it is commonly an anion. The dopant introduces charge carrier adding or removing electrons from/to the polymer backbone and relocalizing as polarons and bipolarons. Applying a potential, the dopants starts moving in or out of the polymer disrupting the neutrality and the charge can pass through the polymer as a polaron or bipolaron ^[70,75-76]. The range of conductivity for conducting polymers in Figure 15.

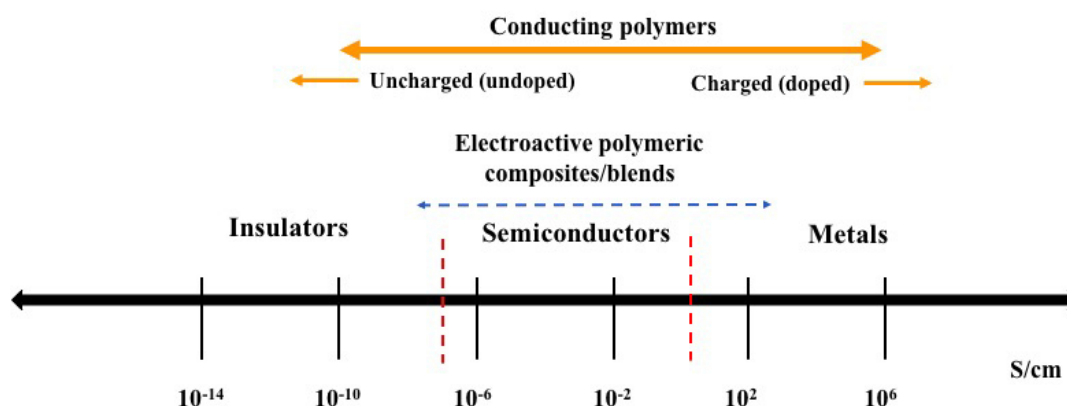


Figure 15. Conductivity range for conducting polymers.

The doping can be two types: p-doping, the polymer is oxidized and have a positive charge and n-doping where the polymer is reduced and has a negative charge. The doping can occur chemically, electrochemically or by photodoping^[77].

Conjugated polymers have attracted attention in hybrid solar cells in order to be implemented as the donor part in the photoactive layer. Optimal conditions are needed for donor polymers which are band gap around 1.5 – 1.6 eV in single junction solar cells, this value can vary in multijunction solar cells, optical absorption is commonly up to 650 nm, high degree of planarity, high hole mobility, etc^[31,78-79]. Most of this characteristics are exhibited by polythiophenes being the typical conducting polymer use in hybrid solar cells recently, analogous selenophenes has started to be studied.

2.11. Polyselenophene

The versatile applications for conducting polymers has made this field grows very fast. The thiophenes are the most studied conducting polymers but since this kind of

polymer exhibit interesting optoelectronic properties, the search for another conducting polymers has been developed. Perhaps, the one of the most interesting polymer is the analogue, selenophene and its derivatives. The structure of selenophene and polyselenophene is given in Figure 16.

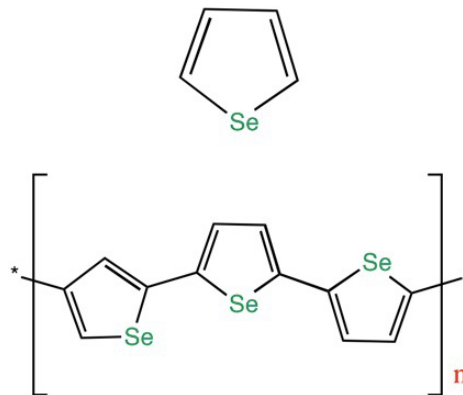


Figure 16. Structure of selenophene and polyselenophene.

The interest in polyselenophene is due to the many advantages that exhibit for:

- a) Intermolecular Se-Se interactions that lead to a wide bandwidth enforcing inter-chain charge transfer,
- b) Selenophenes monomers have lower oxidation and reduction potentials than thiophenes monomers,
- c) Se atom polarizes easier than S atom,
- d) Polyselenophenes should be able to accommodate more charge upon doping than polythiophenes due to Se atom size,
- e) Lower band gap than polythiophenes,
- f) Electrical conductivity should be around $10^{-1} - 10^{-3} \text{ Scm}^{-1}$,
- g) Better control of the planarity in the conjugated backbone and also,
- h) Highly transparent ^[80-84].

The following section is a review on the synthesis of photoactive materials for its application on hybrid solar cells, describing the challenges of developing adequate materials that permits the fabrication of photovoltaic systems with higher efficiencies.

2.12. Literature review

Since Greenham *et al.* studied the first hybrid system of polymer with CdS or CdSe^[85], many reports have focused in the development of organic-inorganic systems in order to find an appropriated active material ^[28, 86-90].

Typically, a hybrid solar cell integrates an organic semiconductor (as a donor) and an inorganic semiconductor (as an acceptor). Photoactive layer absorbs photons generating electron-hole pairs and promoting exciton diffusion towards the electrodes ^[28]. Since only in the interface donor/acceptor can produce free electron charge carriers, it is necessary to increase the interfacial area thus, acceptor and donor should be intimately mixed and therefore, the arrangement between acceptor and donor is crucial for the device performance.

Inorganic materials are metal oxides, III-V, IV, I-III-VI semiconductor or compound semiconductors varying in size and morphology (e.g. nanoparticles, nanorods, nanowires etc.). Nanoscale materials have advantages such as high electron mobility, high electron affinity, good thermal stability and the possibility to have a high interfacial area which as previously mentioned is an important characteristic for efficient exciton

diffusion ^[21,31]. Distinct morphologies have been studied but an interesting nanostructure to provide an ideally straight pathway to carrier transport are 1D ordered nanostructures.

Novel 1D nanostructures, including carbon nanotubes and semiconductor nanowires, have been explored in order to purpose them as the active components in future devices. Nanowires differ from their corresponding bulk counterparts because of their increased surface area, high density of electronic states, diameter-dependent band gap and enhanced exciton binding energy ^[91].

Semiconductor nanowires is an increasing research field due to their interesting physical properties and their wide field of applications in advanced nanodevices. Semiconductor nanowires can be described as quasi-one-dimensional of semiconductor material with diameters of 10 to 100 nm range and with lengths of the order of micrometers ^[92]. According to literature, single nanowires provide to the PVs several key advantages like high-efficiency, robust and integrated nanoscale photovoltaic power sources ^[93]. Nanowires of SnS ^[94], CdS ^[95], ZnO ^[96], ZnS ^[97], CuS ^[98], Cu₂S ^[99], CuO ^[100], FeS₂ ^[101], Bi₂S₃ ^[102] etc., have been investigated with interesting results for their application in photovoltaic applications.

At present, are increasingly efforts for the development of products that will prevent any kind of pollution. For these reason, in this project is purposed the employment of non-toxic nanosemiconductors. In the 80's, FeS₂ (pyrite) represented an interesting semiconductor for photovoltaic due to its environmental compatibility, high absorption

coefficient ($\alpha = 10^5 \text{ cm}^{-1}$), current saturation of 40 to 50 mA/cm² for thickness between 0.2 μm to 1 μm . Although, common impurities appear in FeS₂ (pyrite) when is synthesized, two of them are hexagonal troilite (FeS) and orthorhombic marcasite (FeS₂) with band gaps of 0.04 eV and 0.34 eV respectively, these impurities diminish photovoltaic properties even in trace quantities. Impurities and surface defects promote low open circuit voltage when pyrite is incorporated in solar cells but also, the sulphur deficiency in crystal structure is a reason for low efficiencies. Table 4, shows some reports where pyrite is incorporated in solar cells [103-104].

Table 4. Efficiencies values for solar cells where FeS₂ (pyrite) was incorporated.

Author	Year	Efficiency (%)	System	Reference
Ennaoui <i>et al.</i>	1986	2.8	FeS ₂	[105]
Lin <i>et al.</i>	2009	0.16	P3HT/FeS ₂ (NC)	[106]
Steinhagen <i>et al.</i>	2012	0	P3HT/FeS ₂	[107]
Kirkeminde <i>et al.</i>	2012	1.1	FeS ₂ /CdS	[108]
Richardson <i>et al.</i>	2013	2.89	P3HT:PCBM:FeS ₂	[109]
Khan <i>et al.</i>	2014	0.09-0.67	FeS ₂ :CdSe	[110]
Bhandari <i>et al.</i>	2015	10.6	CdS/CdTe/FeS ₂ /Au	[111]

The following papers detail the challenges for FeS₂ (pyrite) in order to obtain micro and nanostructures, since 1D nanostructures are the principal target of this thesis project the reports are centered in them. Xuefeng *et al.* in 2000, synthesized FeS₂ through solvothermal process where the solvent used was ethylenediamine. According with Transmission Electronic Microscopy (TEM) the as-prepared sample consists in nanorods with diameter about 20-50 nm and lengths of 500- 1000 nm. The formation of FeS₂ nanorods instead of nanowires is due to the intermolecular interactions of the solvents, electrostatic interactions and a supramolecular structure that may provide a template for

the growth of 1D nanostructures. Also, in this work other solvents were tried (1,3-diaminopropane and 1,6-hexanediamine) in both cases one-dimensional nanostructures of FeS₂ were obtained and benzene and toluene were used as solvents as well but in these cases spherical FeS₂ were obtained due to the weak polarity of the solvents, which cannot provide a template for the one-dimensional morphology^[112]. As the aim of this work was to synthesize one-dimensional FeS₂ nanostructures, optoelectronic properties of the nanorods synthesized by solvothermal method are not mentioned and also, the nano-semiconductors did not exhibit an aligned and oriented morphology reducing the high electron mobility around the system. In 2004, Kar *et al.*, carried out the synthesis of highly oriented nanowires using the solvothermal process with ethylenediamine as well. The synthesis was carried out during 6 hours resulting in nanowires of pyrite phase with an overcrowding effect. Nanowires were sonicated in order to obtain them in an individual morphology^[113]. Long times of reaction, equipment acquisition, post-treatment and organic solvents are needed in order to obtain oriented nanowires by solvothermal process.

Another method has been carried out in order to obtain FeS₂ (pyrite) as chemical vapor deposition, thermal sulfidation of iron or hematite and sulfidation reaction with FeCl₂ or FeBr₂. Li *et al.* in 2012, carried out the synthesis of FeS₂ nanowires via thermal sulfidation. This process is carried out under high conditions of pressure and temperature and a special equipment is required. By this technique is also possible to obtain high quality nanowires with little amount of impurities, diameter range between 15-200 nm but

the nanowires are not well-defined and do not exhibit an individual and oriented morphology ^[114].

As previously mentioned, an oriented and vertical morphology is the difficult part to achieve by the methods described before. The template-based synthesis is a conceptually simple and intuitive way to fabricate 1D nanostructures. The main advantage of template-based synthesis over the templateless ones is the control on the morphology, dimensions and compositions of the prepared materials ^[92, 115-116].

In 2005, Wan *et al.*, carried out the synthesis of FeS₂ (pyrite) nanowires by two-step process. First, sulfurizing Fe nanowires and finally, were deposited in the pores of AAO. The obtained FeS₂ nanowires exhibited an ordered array and high density packages. Authors mentioned by this process is difficult that in the nanowire case sulfurize the Fe nanowires to form FeS₂ nanowires due to the little space between Fe nanowires and the AAO walls, resulting with a nanowires mixture of Fe/FeS₂. In order to achieve completely FeS₂ nanowires, the sulfurization process needed 8 h at 450 °C ^[60].

Li *et al.* in 2014, reported the obtaining of iron pyrite nanowires and nanotubes through AAO template synthesis. The obtained nanowires of FeS₂ exhibit uniform lengths and diameters of 200 nm. Their crystal structure was identified as cubic FeS₂ and present band gaps of 0.98 and 1.23 eV. As a hard template was used, the materials obtained showed highly ordered array. This method does not show the appearance of impurities according the X-Ray Diffraction (XRD) analysis ^[117].

Even with FeS₂ (pyrite) nanostructures synthesized through any of the previous methods, pyrite deals with low efficiencies (Table 4). In order to prevent this effect, an option is to enhance its properties in the heterojunction with a wide band gap semiconductor (i.e. ZnO).

ZnO is a semiconductor with a wide range of applications. A number of methods have been used to synthesize ZnO in one-dimensional vertical array in order to improve the electron/donor interface areas including chemical vapor deposition^[118], hydrothermal process^[119], template-based synthesis, electrodeposition etc. High ordered and crystalline nanostructures were obtained. Since chemical vapor deposition and hydrothermal process work under conditions of high pressure and temperature requiring sophisticated equipment is electrodeposition techniques becoming most used to generate ZnO nanowires.

Like FeS₂ nanowires, ZnO nanowires have been synthesized through electrodeposition assisted with AAO templates resulting in pure ZnO nanowires with highly uniform and vertical array, with diameter of 65 nm and lengths of 10 μm. It is remarkable in this process, the potential applied during the synthesis is a factor to consider to obtain ZnO with the desired morphology and optoelectronic properties^[120]. Some variations of this method have been done as the implementation of sodium citrate to control the physical dimensions of ZnO nanowires in order to attend actual demand of better devices^[121].

Properties of semiconductors can be influenced with the incorporation of a second semiconductor, metallic nanoparticles even polymers or another organic compounds. A novel strategy for the enhancement of optoelectronic properties consists is the overgrowth of the surface of the core with a shell of a second semiconductor, resulting in a core/shell arrangement. The core/shell materials that exhibit increasing of photochemical stability and quantum efficiency due to the confinement of the exciton. Researchers have focused in the development of these nanostructures in different morphologies as the next works. Brayek *et al.* in 2014, reported the synthesis of ZnS/ZnO core/shell nanowires. The ZnO NWS were obtained by electrodeposition on ITO glass as working electrode, an Ag/AgCl electrode and platinum electrode were used as reference electrode and counter electrode, respectively. The as-prepared ZnO/ITO sample was immersed in an aqueous solution of Na₂S to convert ZnO to ZnS. De-zhi *et al.* in 2012, reported the formation of a nanocomposite of Cu₂S/tetrapod like ZnO whisker by poliol method where poly(vinyl pyrrolidone) (PVP) was employed as surfactant. XRD patterns for pure Cu₂S and ZnO indicated the cubic and wurtzite structure respectively. Instead, with the nanocomposite is formed, Cu₂S diffraction peaks are absence due to the low amount of Cu₂S. Through the FE-SEM analysis can be observed the effect of concentration of PVP. At low concentration of PVP, many particles and little amount of agglomerates were observed on the surface of ZnO. But with a high concentration of PVP the nanoparticles are not deposited on ZnO surface. In the development of these nanostructures, it is observed the influence of the core for the optical absorption and at the same time the core influences separation and carrier collection while, the shell thickness influences carrier collection.



Thus, it can be assumed that nanowires in core/shell nanostructure provide an interesting array to synthesize semiconductor materials ^[122-124].

In section x was mentioned the importance of conducting polymers and their interesting optoelectronic properties, focusing in polyselenophene family which have a number of papers as Patra *et al.* in 2014, reported the comparison between PEDOT and PEDOS where the last one exhibit a more rigid structure, lower band gap, stability, a more rigid backbone, transparency and higher conductivity due to its electron donating characters, low aromaticity, oxidation potential, electronegativity and polarizability ^[125]. Nowadays, new and non-toxic materials for energy conversion and storage are studied in order to provide the enough energy with the less impact to the world. In the case of polyselenophene can be doubted the inclusion of this material as part in the photoactive layer but according the literature selenophene heterocycles are an important class of compounds for biological and medical studies ^[126].

2.13. Scientific contribution

Core/shell nanowires of FeS₂/ZnO coupled into a polymeric matrix of a polyselenophene for its application in hybrid solar cells.

2.14. Hypothesis

Core/shell nanowires of FeS₂/ZnO coupled into a polymeric matrix of a polyselenophene show suitable morphological array and optoelectronic properties for its application as photoactive layer in hybrid solar cells.



2.15. Goals and objectives

General objective:

Synthesizing, coupling and characterizing core/shell nanowires of FeS₂/ZnO into a polymeric matrix of a polyselenophene for its application as photoactive layer in hybrid solar cells.

Specific objectives:

1. Synthesizing core/shell nanowires of FeS₂/ZnO through electrochemical method assisted by AAO template.
2. Characterizing semiconductor nanowires by UV-Vis, PL, FE-SEM (EDS), VC and TEM.
3. Synthesizing a novel derivative of polyselenophene through aldol condensation.
4. Characterizing conducting polymer by UV-Vis, FTIR, VC and DTA-TGA.
5. Coupling semiconductor nanowires into a conducting polymeric matrix of a polyselenophene.
6. Characterizing hybrid material by UV-Vis, FTIR, DTA-TGA, FE-SEM, TEM, VC and EIS.

Academic goals:

1. Developing expertise in the field of materials chemistry.
2. Developing a new methodology to obtain one-dimensional core/shell nanostructures through electrochemical assisted method.
3. Spreading results with papers and participating in international congresses.
4. Publishing the results obtained in an indexed journal by JCR.
5. Obtaining the degree of Master of Science.

Chapter 3
Materials and Methods

It is described in this chapter the methodology for the synthesis of FeS₂ (pyrite) through microwave method. It is also mentioned the synthesis and characterization of ZnO nanotubes by immersion method and its subsequently coupling with FeS₂ in order to obtain FeS₂/ZnO core/shell nanowires. As for the polymer synthesis is described the method of obtaining and the subsequently incorporation of FeS₂/ZnO inside the polymeric matrix. Finally, the characterization techniques are also mentioned in order to evaluate its optical, morphological and electrochemical properties.

3.1. AAO templates fabrication

Since the morphology desired for the core/shell is a one-dimensional array through electrodeposition method assisted by AAO templates, it is described firstly in this section the synthesis of templates.

AAO templates synthesis corresponds for a 5-step process which are:

1. Aluminum cleaning.
2. First anodization.
3. Etching.
4. Second anodization.
5. Pore widening.

AAO templates by itself are not conductive. For this reason, is necessary an extra process to make them conductive. It requires the deposition of a layer of a conductive material as Au or Ag with the previous removal of the barrier layer.

3.1.2. Methodology for AAO templates

Aluminum cleaning: for the suitable synthesis of AAO templates was necessary to clean the surface of Al foil in order to remove organic waste and obtain a smooth surface of the sample. Firstly, it was rinsed in water in an ultrasonic bath for 10 minutes then, it was cleaned mechanically with polishing wax to remove dust and scratches. Finally, Al foil was electropolished in order to obtain a smooth and shiny surface.

First anodization: a solution of $\text{H}_2\text{C}_2\text{O}_4$ 0.3 M was added in the cell. Al foil was placed at the bottom of the cell and the wires were connected at positive and negative terminal. The distance between electrodes were 3 cm with a surface of Al foil of 0.8 cm^2 in contact with oxalic solution. The first anodization lasted 2 hours at 40 V.

Etching: The oxide layer that remains in the templates was etched with a solution of 1.8wt% H_2CrO_4 and 5wt% H_3PO_4 . The sample was drawn in the solution during 40 minutes at 65 °C.

Second anodization: As the first anodization, the Al foil was placed at the bottom of the cell with oxalic acid 0.3 M. The distance between electrodes were 3 cm with a surface of

Al foil of 0.8 cm^2 in contact with oxalic solution. The process lasted 2 hours at 40 V.

Pore widening: the template is drawn in a 6 wt% solution of H_3PO_4 at $35 \text{ }^\circ\text{C}$. The time is key during this process since the template can be etched so quickly. The time was varied between 5-10 minutes even it was omitted.

Figure 17, illustrates the methodology for AAO templates fabrication.

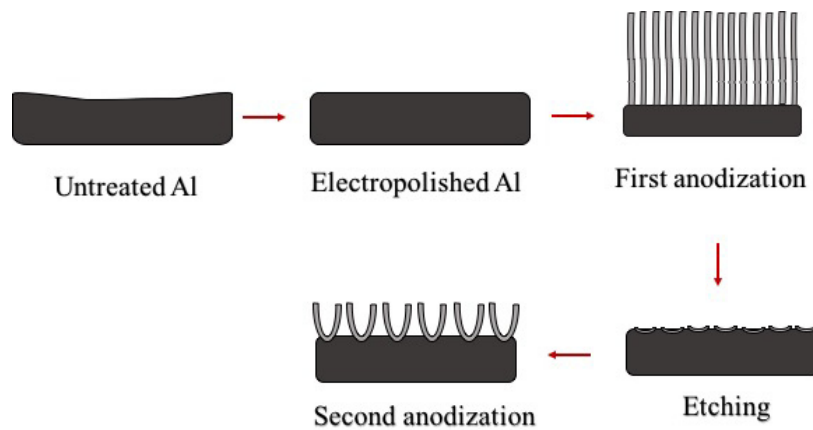


Figure 17. Methodology for the fabrication of AAO templates.

3.1.3. Making AAO templates conductive

AAO template as mentioned before is not conductive by itself due to the presence of barrier layer. This barrier does not allow the current pass through the channels. Thus, this layer must be removed in order to electrons can reach the bottom of the channels. In this work, a solution of 0.1M CuCl_2 in $\text{H}_2\text{O}/\text{HCl}$ mixture (2:1) was used to remove barrier layer. Subsequently, the pore widening was carried out with 5wt% H_3PO_4 . Without the

barrier layer, a layer of Au was deposited by sputtering using a Denton Vacuum Desk V. The removal process is illustrated in Figure 18.

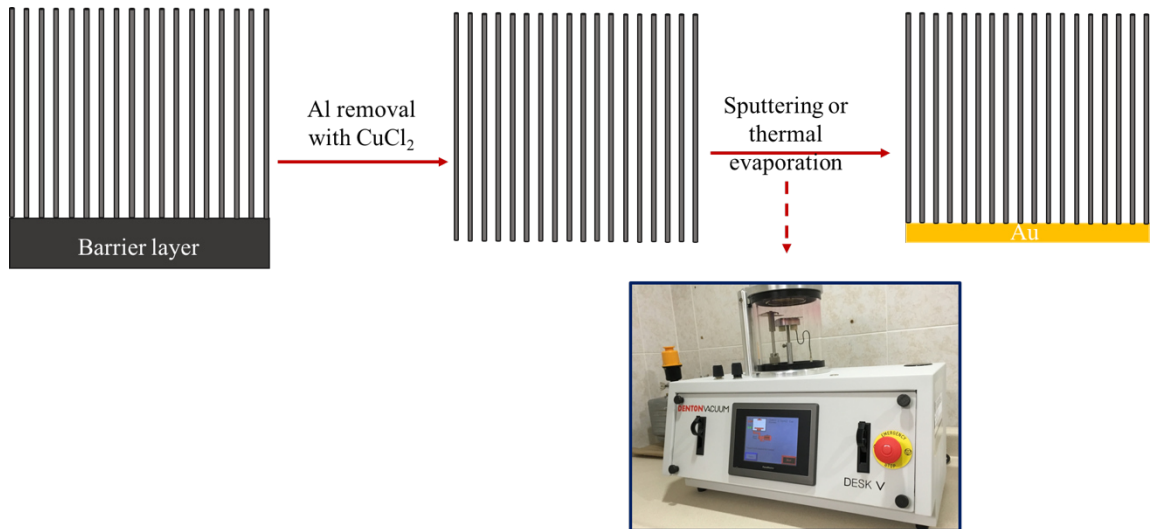


Figure 18. Removal process and Au deposition for AAO templates.

3.1.4. Cell design for AAO templates

Cell design is given in Figure 19, which was used for the fabrication of the templates. The cell design corresponds to a previous work carried out in the research group.

In a general way, the cell body was a PVC tube in order to avoid corrosion for the electrolyte. In the bottom was placed the Al pure foil that was in contact with the acidic solution and connected in the positive terminal to the power supply. The negative terminal corresponded to an Al commercial sheet since Pt is an expensive material to be used in the anodization process. During the synthesis was necessary to stir the solution in order to

distribute the temperature around the cell. In order to maintain the temperature during all the process, it was used a Peltier at the bottom of the cell and above of a ventilator.

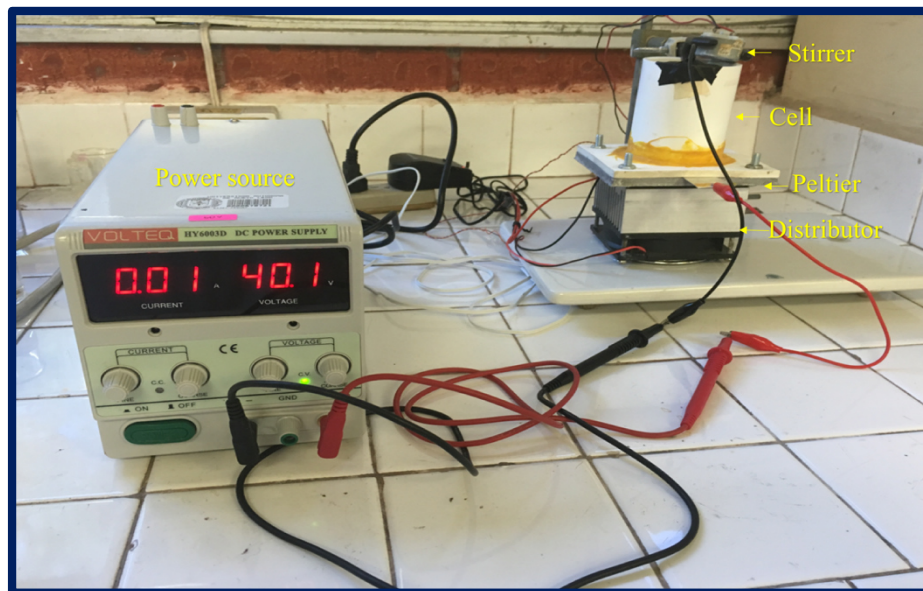


Figure 19. Composition of the cell for the fabrication of templates.

3.2. Synthesis of ZnO nanotubes by immersion method

Synthesis of ZnO nanotubes was carried out by immersion method of AAO templates, purposed by Liu *et al.* ^[127] and the optoelectronic properties were also evaluated. 0.35 g of $\text{Zn}(\text{O}_2\text{CCH}_3)_2$ was dissolved in 20 mL of ethanol and stirred until a clear solution was obtained and then 0.08 g of KOH was added. The mixture was ultrasonicated until a white was obtained. The AAO template was immersed into the suspension for 1 min and dry at room temperature for 30 min and undergone a heat-treatment at 600 °C for 4 h. Experimental procedure for ZnO nanotubes is given in Figure 20.

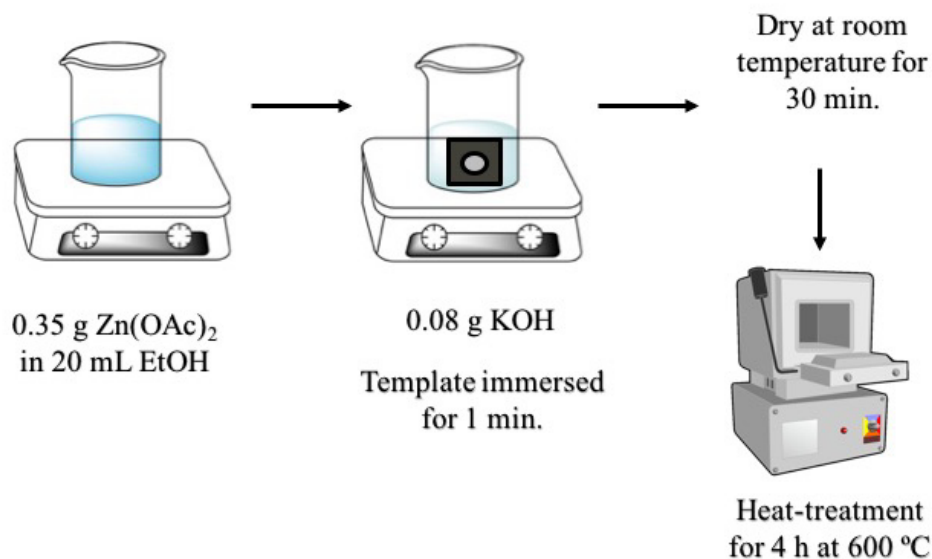


Figure 20. Experimental procedure for ZnO nanotubes.

3.3. Synthesis of FeS_2 nanowires by microwave heating method

For the synthesis of FeS_2 was studied distinct conditions in order to understand the mechanism of this material and to find the best conditions to carry out the synthesis through microwave heating method. Optoelectronic, structural and morphological properties were studied.

1 mmol of anhydrous FeCl_2 and 4.5 mmol of sodium thiosulfate were dissolved in 50 mL of ethylenglycol (EG) under magnetic stirring. Then 4 mmol mercaptoacetic acid (MPA) was added to the solution under continuous stirring. Finally, deionized water was poured into the solution. Microwave heating was performed on the reaction mixture in cycles of 10 s on and 30 s off at 100% microwave power (1000 W, 2.45 GHz). Solutions reacted with a total heating time of 150 s or 210 s. Reaction finalized when grayish-black

powder appears. The end product was centrifuged and washed several times with deionized water, ethanol and acetone. In order to purify the black powder was washed with HCl 2N. Finally, the product was dried under N₂ flux at room temperature for 15 minutes. Representation of the experimental procedure for microwave synthesis is given in Figure 21.

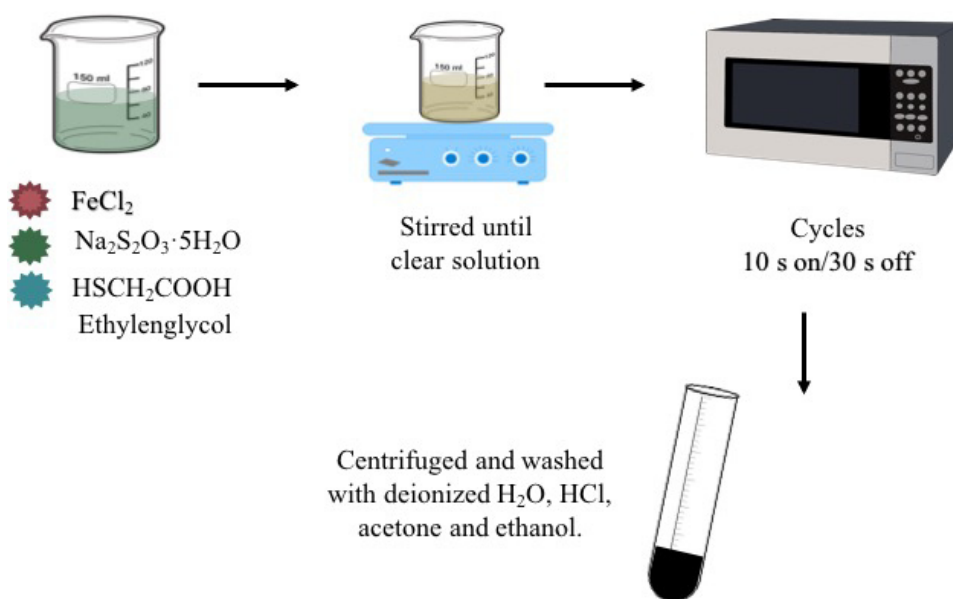


Figure 21. Experimental procedure for the synthesis of FeS₂.

3.4. Synthesis of 2,5-Selenophenedicarbaldehyde by Vilsmeier-Haack reaction

In a reaction vessel is added 3.81 mmol of selenophene and 5.34 mmol of DMF under inert atmosphere of N₂. Subsequently, 5.34 mmol of POCl₃ is added dropwise under magnetic stirring at 70 °C for 30 minutes. After that time, ice is poured into the mixture and neutralized with sodium acetate. Extractions with diethyl ether was carried out in order to purify the target compound. The reaction was monitored through thin layer

chromatography (TLC) with a mobile phase of hexane:ethyl acetate (1:1). The Figure 22, shows the corresponding reaction for this procedure.

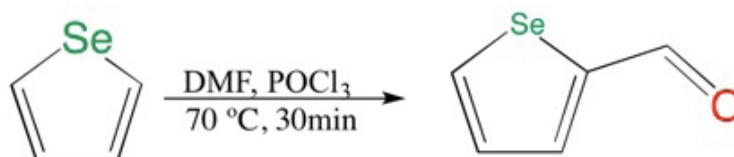


Figure 22. Reaction for the synthesis of 2-selenophenedicarbaldehyde.

In order to synthesize 2,5-selenophenedicarbaldehyde, it was carried out a second Vilsmeier-Haack reaction with the previous 2-selenophenedicarbaldehyde obtained. 0.5 g of 2-selenophenedicarbaldehyde was placed under N_2 atmosphere with 6.28 mmol of DMF and added 6.28 mmol of $POCl_3$ dropwise. The reaction mixture was kept at 70 °C for 30 minutes. The procedure to neutralized and for the extraction was the same for 2-selenophenedicarbaldehyde. Finally, the product was filtered and recrystallized with ethanol. The Figure 23, illustrates the reaction corresponding for this procedure.

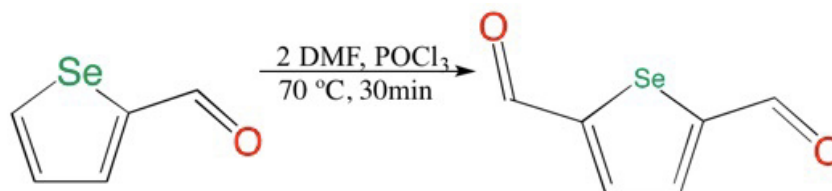


Figure 23. Reaction for the synthesis of 2,5-selenophenedicarbaldehyde.

Another procedure was purposed for the synthesis of 2,5-selenophenedicarbaldehyde. A mixture of 2-selenophenedicarbaldehyde (0.50 g) and DMF (12.57 mmol) was placed in a two neck round-bottom flask. The vessel was under N_2 atmosphere while the reaction took place. $POCl_3$ was added dropwise. After the

addition was completed, the mixture was kept under stirring and heating at 70 °C for 30 minutes. After reaction, solution was poured into a certain amount of ice and neutralized with sodium acetate. The solution was extracted with diethyl ether. Figure 24, shows the reaction that took place.

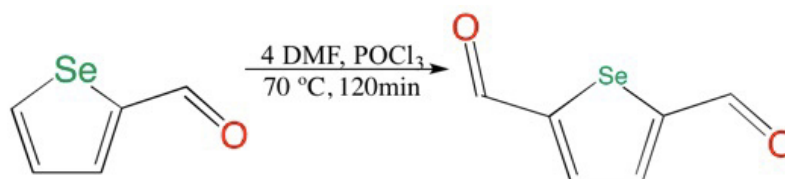


Figure 24. Second reaction for the synthesis of 2,5-selenophenedicarbaldehyde.

3.5. Synthesis of a polyselenophene by aldol condensation

0.017 g of NaOH and 1.15 mL of ethanol were added in a reaction vessel under reflux and kept at 40 °C. 0.156 g of a mixture of 2-selenophenedicarbaldehyde/2,5-selenophenedicarbaldehyde were dissolved with 0.8 ml of ethanol 50%. Subsequently, 0.025 g of acetone in 0.2 mL of ethanol 50% were added. The reaction took place during 15 minutes. The end product was centrifuged and washed with deionized water. Finally, the product was dried at 70 °C for 2h. Polymerization reaction is given in Figure 25.

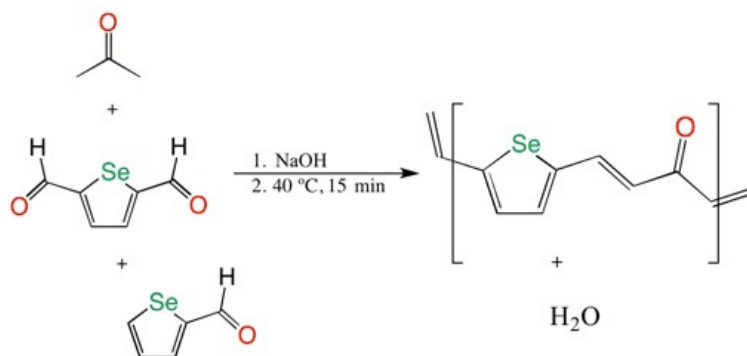


Figure 25. Polymerization reaction of 2,5-selenophenedicarbaldehyde.

3.6. Characterization techniques

The electromagnetic spectrum represents the total radiation spectrum. Most of the interactions between atoms and molecules with the distinct radiations can be measured with different sensing instruments. In Figure 26, illustrates the electromagnetic spectrum, the Ultraviolet-visible (UV-Vis), and Infrared fundamentals will be detailed in the following sections.

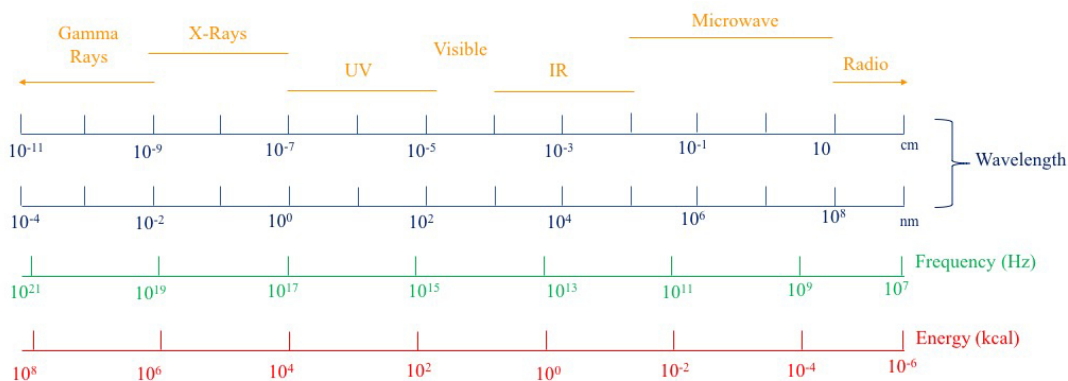


Figure 26. Electromagnetic spectrum.

3.6.2. Ultraviolet-visible spectroscopy (UV-Vis)

Ultraviolet-visible spectroscopy involves the spectroscopy of photons in UV-visible region. This region includes wavelength from 10 to 780 nm and the limit between both of them is around 390 nm. UV-visible radiation originates due to the rearrangement of outer and inner electrons.

Mainly, three process are involved in UV-Vis spectroscopy: reflection, absorption

and transmission of radiation ^[128].

- **Reflection:** a portion of the radiation returns to the space from which it was emitted. Reflection may be specular, diffuse or some combination of the two.

- **Absorption:** part of the radiation to change into a different form of energy, usually heat. This third major process is known as absorption. Its associated quantity, absorptance may be determined using the equation:

$$\alpha = \frac{\phi_a}{\phi_i} \quad \text{eq. (2)}$$

where ϕ_a represents the amount of incoming radiation absorbed by the material.

- **Transmission:** refers to an event in which the radiant flux incident to the surface of a sample departs from a different surface (usually from the opposite side of the sample).

UV-Vis spectrometer is an equipment that works with a double-beam where one beam reaches the reference and a second one reaches the sample, being 100% of transmission the reference value and the measurement is a ratio between both intensities ^[129].

In addition, UV-Vis analysis allows the study of the band gap for semiconductors, transitions of nanomaterials, phenomena as localized surface plasmonic resonance (SPR), size effects, kinetics of growth of nanostructures, concentration in the degradation of pollutants or dyes, etc. ^[130].

3.6.3. Photoluminescence (PL)

Luminescence involves two process: the absorption of energy from a light source and the subsequent emission of light. It includes the radioluminescence, electroluminescence, chemiluminescence, photoluminescence and bioluminescence depending of the energy source.

Photoluminescence takes place when the external energy comes from ultraviolet, visible or infrared light and emission occurs. The ultraviolet and visible regions of the spectrum are of most interest in fluorimetry since the absorption in these regions causes the excitation of the outermost electrons of the molecule ^[131].

An excitation wavelength is selected by one monochromator, and luminescence is observed through a second monochromator, usually positioned at 90° to the incident light to minimize the intensity of scattered light reaching the detector. If the excitation wavelength is fixed and the emitted radiation is scanned, an emission spectrum is produced ^[132].

Several information may be obtained by PL. Presence of impurities and its dependence on the level of photo-excitation is related to the recombination process. Also, PL is very sensitive to surface effects or adsorbed species of semiconductor particles allowing the study of electron-hole surface process ^[133].

3.6.4. Fourier transform infrared spectroscopy (FT-IR)

Infrared spectroscopy is a technique based on the vibrations of the atoms of a molecule. An infrared spectrum is commonly obtained by passing infrared radiation through a sample and determining what fraction of the incident radiation is absorbed at a particular energy. The energy at which any peak in an absorption spectrum appears corresponds to the frequency of a vibration of a part of a sample molecule. The infrared spectrum can be divided into three main regions: the *far-infrared* ($<400\text{ cm}^{-1}$), the *mid-infrared* ($4000\text{--}400\text{ cm}^{-1}$) and the *near-infrared* ($13000\text{--}4000\text{ cm}^{-1}$) [134].

The radiation emerging from the source is passed through an interferometer to the sample before reaching a detector. Upon amplification of the signal, in which high-frequency contributions have been eliminated by a filter, the data are converted to digital form by an analog-to-digital converter and transferred to the computer for Fourier-transformation [135].

FT-IR spectrum covers the interpretation of the vibrations as bands that appear which, are assigned to a particular bonding of a molecule, known as group frequencies. This information allows a partial recognition of the target molecule supporting information is needed in order to elucidate a molecule.

3.6.5. X-Ray diffraction (XRD)

X-rays refer to the electromagnetic radiations with wavelength of 10^{-3} nm to 10 nm. X-ray diffraction is essentially a scattering phenomenon in which a large number of atoms are involved. Since the atoms in a crystal are periodically arranged, the X-rays scattered by these atoms can be in phase and constructively interfere in a few directions [136].

X-rays with wavelengths below 0.1–0.2 nm are called hard X-rays, while those with longer wavelength are called soft X-rays. The X-rays utilized for materials analysis are hard X-rays. First, hard X-rays are deeply penetrating into all substances, although the penetration depth varies with the substance. In particular, hard X-rays have wavelengths similar to the size of atoms. Therefore, they can be diffracted by atoms periodically arranged within the substance. Monitoring the diffraction direction and intensity allows the internal structure of crystalline matters to be revealed at the atomic level [137].

The general relationship between the wavelength of the incident X-rays, angle of incidence and spacing between the crystal lattice planes of atoms is known as Bragg's Law, expressed as:

$$n \lambda = 2d \sin\theta \quad \text{eq. (3)}$$

where n is the "order" of reflection, λ is the wavelength of the incident X-rays, d

is the interplanar spacing of the crystal and θ is the angle of incidence ^[138].

X-rays can also reveal various information on the materials, including crystal structure, phase transition, crystalline quality, orientation, and internal stress.

3.6.6. Scanning Electron Microscopy (SEM)

SEM uses a focused beam of high-energy electrons to generate a variety of signals at the surface of solid samples. Areas ranging from approximately 1 cm to 5 microns in width can be imaged in a scanning mode using conventional SEM techniques (magnification ranging from 20 X to approximately 30,000 X, spatial resolution of 50 to 100 nm) ^[139].

SEM uses an electron beam emitted from an electron gun which goes through electromagnetic lenses as condenser lenses and apertures in order to generate a variety of signals at the surface of solid specimens. The signals give different information about the specimen due to the interactions between the electron beam and the sample ^[140].

The SEM is used to generate high-resolution images of shapes of objects (SEI) and to show spatial variations in chemical compositions: 1) acquiring elemental maps or spot chemical analyses using EDS, 2) discrimination of phases based on mean atomic number (commonly related to relative density) using Backscattered electron images (BSE), and 3) compositional maps based on differences in trace element using cathodoluminescence



(CL). The SEM is also widely used to identify phases based on qualitative chemical analysis and/or crystalline structure. BSE can be used for rapid discrimination of phases in multiphase samples. SEMs equipped with diffracted backscattered electron detectors (EBSD) can be used to examine microfabric and crystallographic orientation in many materials ^[141].

3.6.7. Transmission Electron Microscopy (TEM)

TEM is a very powerful tool for material science. A high energy beam of electrons is shone through a very thin sample, and the interactions between the electrons and the atoms made possible to study growth of layers, their composition and defects in semiconductors. Transmission electron microscopy (TEM) provides a wide range of methods to study the morphology, the crystal structure and perfection, the chemistry, and the magnetic and the electronic properties of the matter at the highest spatial resolution. High resolution (magnification of 500–1,000,000X) allows to analyze quality, shape, size and density of quantum wells, wires and dots ^[142].

TEM instrumentation is similar as the SEM's although the visible light is replaced with electron beam ($\sim 1\text{--}10 \text{ \AA}$), which across the specimen. Intermediate lenses and selected area aperture are part of them as well. When the specimen is scanned, data as emitted X-rays, secondary electrons or backscattered electrons are acquired. The information is detected with a moveable detector at the bottom of the microscope column.

Vacuum environment is needed in order to avoid collisions between high energy electrons and air molecules ^[143].

Transmission electron microscopy (TEM) techniques, including scanning transmission electron microscopy (STEM); X-ray energy-dispersive spectroscopy (EDS); electron energy-loss spectroscopy (EELS); selected area (SA), nanobeam (NB), and convergent-beam (CB) electron diffraction (ED); electron tomography (ET); and electron holography, are powerful in characterizing for nanomaterials ^[144].

3.6.8. Cyclic Voltammetry (CV)

Voltammetry includes: potential step voltammetry, linear sweep voltammetry and cyclic voltammetry, the three techniques consist in to apply a voltage to the electrode and the corresponding current is monitorized by an electronic system.

Potentiostat applies an initial potential (E_i) ramp to the working electrode immersed in an unstirred solution and measuring the resulting current, at the end of its linear linear sweep, the scan reverses and usually stop at initial potential E_i ^[145].

Important information is required in order to understand the electrochemical process involved in each system ^[146]:

- a) Location of the forward and reverse on the potential axis (E_p and ΔE_p).
- b) Ratio of currents observe on the reverse and forward scans.

c) Dependence of peak currents on the scan rate (i_p vs. $V^{1/2}$).

The potentiostat, where the excitation signal is produced by a waveform generator which, it is applied to an electrochemical cell, the resulting current is measured by a current-to-voltage converter and a XY recorder or oscilloscope displays the voltammogram. CV takes place in a three-electrode cell, where the potential is applied between the working electrode and a reference electrode. As working electrode distinct substrates have been used (conductive glass, metal substrates, etc) while, reference electrode is typically a saturated calomel electrode (SCE) or a silver/silver chloride electrode (Ag/AgCl). The third electrode is the auxiliary electrode, usually is a platinum wire (Pt) ^[147].

During the CV, a cycling potential of an electrode take place. However, scan rate is mainly the principal parameter to apply in CV, commonly scan rates faster than 100 V/s are rarely practical due to iR drop and charging current.

CV is a useful technique for kinetics, rates and mechanisms. In materials science, CV usually allows the study of band gap through the energy levels of organic and inorganic materials, the growth mechanism of nanostructures, the presence of intermediates in oxidation-reduction reactions, diffusion coefficient and so on ^[148-149].

3.6.9. Electrochemical Impedance Spectroscopy (EIS)

Electrochemical Impedance is the measured of current through an electrochemical cell when is applied an AC potential. The current signal can be analyzed as a sum of sinusoidal functions (Fourier series). Usually, a small excitation signal is used for the measuring with a pseudo-linear response ^[150].

Impedance is the ability of a circuit element to resist the flow of electrical current, Ohm's law describes it:

$$R = \frac{E}{I} \quad \text{eq. (4)}$$

where R is the resistance of the circuit, E is the potential applied and I the current.

But Ohm's law is limited to only one circuit element-ideal resistor. An ideal resistor should have the properties of following Ohm's law at all current and levels, resistance value independent of frequency and AC current and voltage signals are in phase with each other. Since real circuits are more complex, impedance as mentioned above measure the ability to resist the flow of electrical current without the limitation of an ideal resistor. Thus, EIS is technique for the characterization of complex non-linear process using Faraday's law ^[151].

The Nyquist, Bode phase and Bode modulus plots are the most often used data plots in impedance spectroscopy. These plots are representations of calculated (processed)



data. Complex plane (Nyquist) plots are the most often used in the electrochemical field because they allow for an easy prediction of the circuit elements. Nevertheless, Nyquist plots allow for an easy relation to the electrical model, while Bode plots are useful in circuit analysis ^[152].

3.6.9. Differential Thermal Analysis-Thermogravimetric Analysis (DTA-TGA)

Thermal analysis consists in a group of techniques which measure the change of the properties of a certain material under temperature change. Includes different methods but in this thesis is referred only the methods of differential thermal analysis, thermogravimetric analysis and differential scanning calorimetry.

Usually, DTA and TGA methods are runned at the same time since thermal events can be related with losses of mass and give a more accurate information about process of dehydration, decomposition, desorption, oxidation, crystallinity, purity, transition temperatures, volatile content, thermal stability, etc ^[153].

DTA consists in the temperature difference between the sample and an inert reference as function of identical temperature cycles (or time). Temperature difference indicates a heat exchange qualitatively and allowing the identification of exothermic or endothermic events. While, TGA covers the change of mass of a sample on heating measures mass changes in a material as a function of temperature or time under controlled atmosphere ^[154-155].

The instrumentation consists of a sample holder, thermocouples, sample containers, a ceramic or metallic block, a furnace, a temperature programmer and a recording system. When the furnace heating begins, the reference and sample start heating with a slight delay depending on their respective heat capacity and eventually heat up in according to the furnace temperature. The difference of temperature changes until a static state is reached after the heating begins and after achieving stability reaches a set amount compliant with the difference in heat capacity between the sample and the reference ^[156].

3.6.10. Differential Scanning Calorimetry (DSC)

DSC is a thermoanalytical technique where is measured the difference in the amount of heat flow of a sample and a reference as a function of time, providing quantitative or qualitative data on endothermic or exothermic processes. Since the DSC is at constant pressure, heat flow is equivalent to enthalpy changes:

$$\Delta \frac{dH}{dt} = \left(\frac{dH}{dt} \right)_{sample} - \left(\frac{dH}{dt} \right)_{reference} \quad \text{eq. (5)}$$

which can be positive or negative. In an endothermic process, such as phase transitions, heat is absorbed and, therefore, heat flow to the sample is higher than the reference. While, exothermic process, such as crystallization, some cross-linking processes, oxidation reactions, and some decomposition reactions have negative heat flow ^[157].



Calorimeters consists of a sample and reference holder. Reference holder should be an inert material such as alumina or just an empty aluminum pan. Pans can be Al, Cu, Au, Pt, alumina, or graphite and need to be chosen in order to avoid reactions with samples. Temperatures can range from -120 °C to 725 °C, though an inert atmosphere is required above 600 °C. Atmospheres can be nitrogen, air, oxygen, argon, vacuum or mixtures of gases. The computer is used to monitor the temperature and regulate the rate at which the temperature of the pans changes. A typical heating rate is around 10 °C/min.

[158]

DSC allows the study of glass transition, melting points, crystallization times and temperatures, heats of melting and crystallization, oxidative stabilities, heat capacity, thermal stability, polymorphism, compositional analysis and so on ^[159].

Chapter 4

Results & Discussions

The developing of high-purity FeS₂ (pyrite) through methods is currently a challenge for researchers. It is required an extensive study of key parameters as temperature, pH, ratio of Fe/S and also, the source of Fe and S, for the adequate synthesis of this system due to the presence of many polymorphs (pyrrotite, marcasite, mackinawite, etc). In the present chapter is described the results of this thesis and is discussed in the following way: AAO templates fabrication, synthesis of ZnO nanotubes and FeS₂ nanowires, synthesis of a polyselenophene and finally, the coupling between inorganic-organic materials.

4.1 AAO templates fabrication

In order to evaluate the importance of the first-anodization a previous experiment was carried out at the same conditions mentioned in the methodology chapter with the difference the experiment lasted 30 minutes. Figure 27 shows the SEM images obtained from the sample. It can be observed the pores are randomly distributed and are not uniform causing the templates exhibited a poor quality that make not a suitable substrate for the synthesis. It is reported in literature the first-anodization is the pre-patterning process thus, the control of time is key to obtain high quality templates. In Figure 28, the templates were fabricated during 2 h allowing the pores growth uniformly and with a better distribution than before.

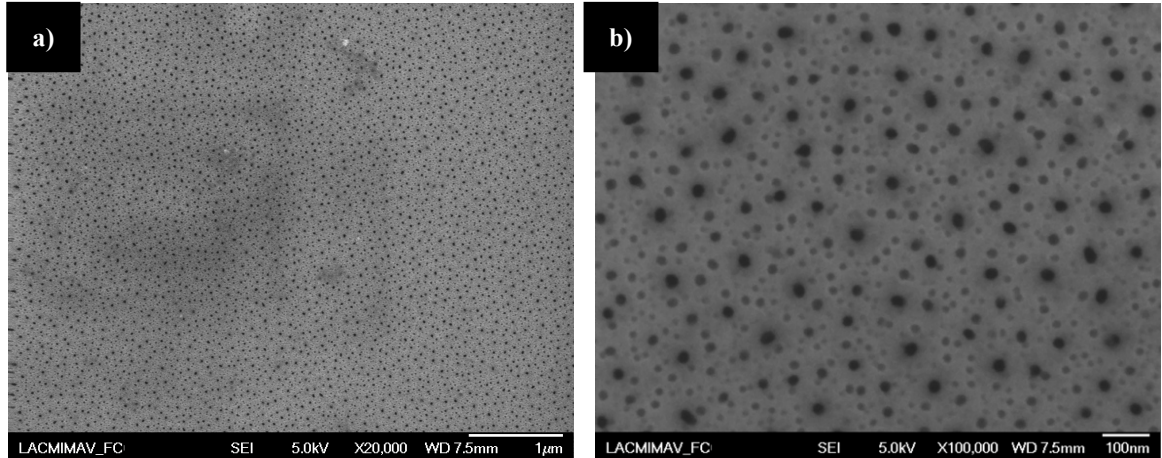


Figure 27. SEM micrography, first anodization: 30 min a)X20,000 and b)X100,000

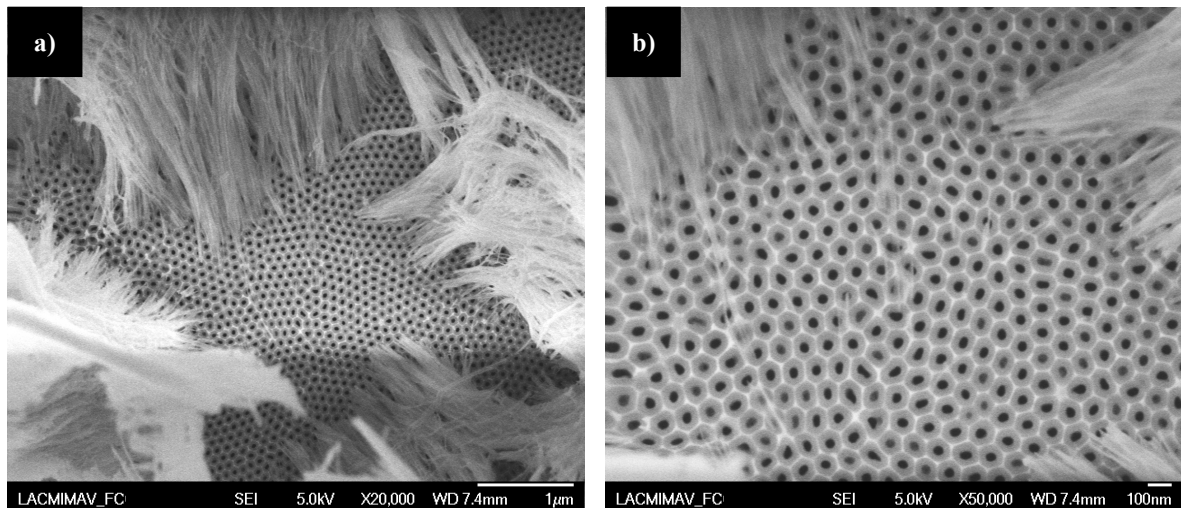


Figure 28. SEM micrography , first anodization: 2h a)X20,000 and b) X50,000.

The etching process should last $\frac{2}{3}$ time of the first anodization, for this reason the following experiments were of 2 h of first-anodization, 40 minutes of etching and 2 h of second-anodization since a previous work in the research group evaluated the optimum conditions for the second-anodization were also, the time is an important factor in the obtaining of a certain thickness of the barrier layer of the AAO template. Also, the second-anodization allows the correct ordering of the pores as can be seen in Figure 29.

Depending the final application of the nanomaterial synthesized with the templates is the size of pore which it is desired for, since the size of pores can increase with H_3PO_4 5%wt at 35 °C. In Figure 29, the SEM image shows the increasing of the size of the pores with 10 minutes of etching. If the time is longer, the pores will grow until they merge together and making the template unusable. The control of time is important in order to obtain one-dimensional material with certain diameter and length.

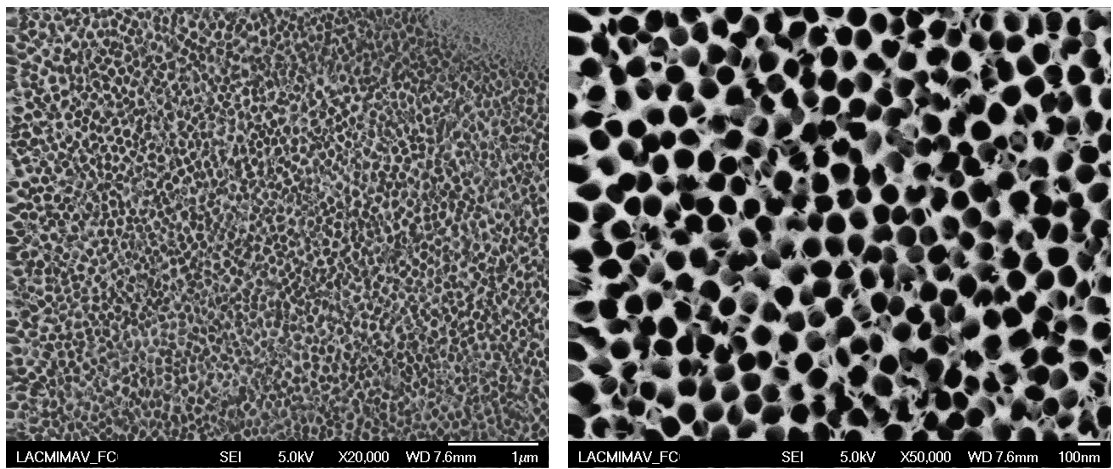


Figure 29. SEM micrography, first and second anodization 2h, a) X20, 000 and b) X50,000.

4.2 ZnO nanotubes

Figure 30 shows the UV-Vis spectrum of ZnO nanotubes inside the pores of AAO. Due to the fact ZnO nanotubes are still embedded in the template, it is the main reason ZnO absorption cannot be seen clearly since it is overlapped with aluminum oxide. Instead in Figure Xb, UV-Vis spectrum shows an optical absorption for ZnO nanotubes around 390 nm and an estimated of $E_g = 3.18$ eV.

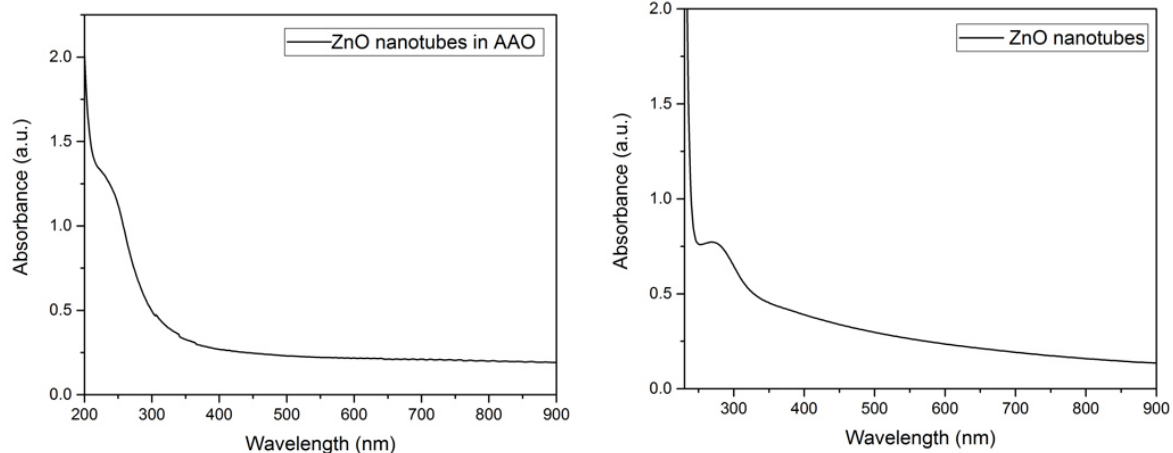


Figure 30. Optical absorption for ZnO nanotubes a) embedded AAO template and ZnO released.

Figure 31 shows the PL emission peaks for ZnO nanotubes. ZnO exhibits peaks near 560 nm and 620 nm. The PL peak located at 560 nm originates from combined oxygen vacancies. According to literature the relation between both peaks have an effect over the morphology of the semiconductor so it could be attributed to behavior of a 1D system.

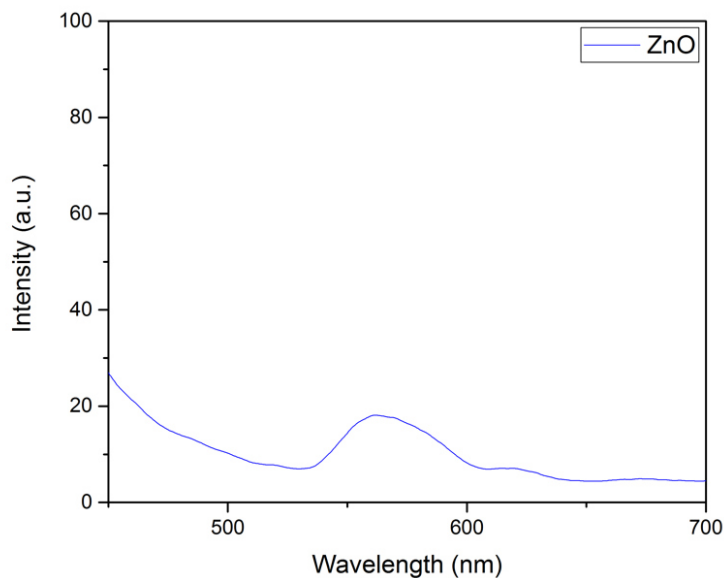


Figure 31. Emission spectra for ZnO nanotubes.

4.3. FeS₂ (pyrite)

Since the synthesis of FeS₂ represents a challenge, it was studied different parameters in order to find the adequate conditions in order to obtain FeS₂ (pyrite) without impurities of FeS and FeS₂ (marcasite). The mechanism proposed by Wang *et al.*, was used as reference for the synthesis under microwave heating. The mechanism is illustrated in Figure 32 where the ethylenglycol is used as a medium for the formation of S²⁻ and the subsequent reaction will produce FeS but a second reaction between FeS and S²⁻ in order to obtain FeS₂. Although, ethylenglycol not only can be used as solvent but also as medium to avoid the formation of iron oxides without the use of an inert atmosphere.

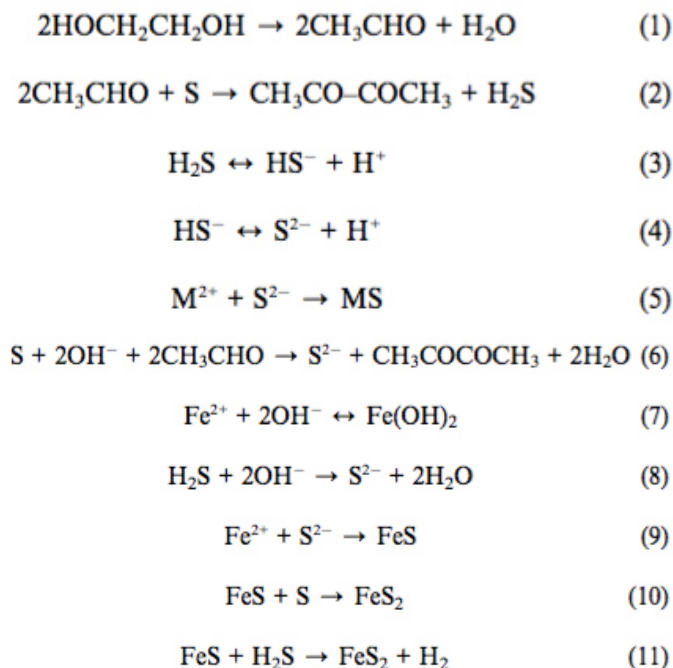


Figure 32. Mechanism for FeS₂ synthesis.

Table 5 shows different conditions evaluated for pyrite synthesis where it can be concluded the need for an stabilizer in order to produce pyrite and avoid polymorphs formation also, the stabilizer can play the role of a double source of S since the formation of S^{2-} can occur more rapidly. Besides, iron source allows the formation preferently of pyrite instead of polymorphs when iron chlorides are added in the reaction vessel.

Table 5. Parameters evaluated for the synthesis of FeS_2 (pyrite).

Experiment	Source of Fe	Source of S	Solvent	HCl	XRD
1	$Fe(NO_3)_3 \cdot 9H_2O$	TAA	EG/ H_2O	x	polymorph
2	$Fe(NO_3)_3 \cdot 9H_2O$	MPA	EG/ H_2O	x	polymorph
3	$Fe(NO_3)_3 \cdot 9H_2O$	TAA/MPA	EG/ H_2O	x	-
4	$FeCl_3$	TAA	EG/ H_2O	x	polymorph
5	$FeCl_3$	MPA	EG/ H_2O	x	polymorph
6	$FeCl_3$	TAA/MPA	EG/ H_2O	x	polymorph
7	$FeCl_3$	Sodium thiosulfate	EG/ H_2O	x	-
8	$FeCl_2$	TAA	EG/ H_2O	x	-
9	$FeCl_2$	TAA/MPA	EG/ H_2O	x	-
10	$FeCl_2$	Sodium thiosulfate	EG/ H_2O	x	-
11	$FeCl_2$	Sodium thiosulfate /MPA	EG/ H_2O	✓ □	Pyrite

Even when all the previous conditions were used for the synthesis of FeS_2 (pyrite), it is important to purify the end product in order to wash any impurities with HCl since

pyrite can not be dissolved in this acid. The corresponding characterization of this semiconductor is discussed in the following section.

Figure 33 shows the XRD pattern for FeS₂ where crystal lattice corresponded to cubic system and no impurities of FeS or FeS₂ (marcasite) appeared. The lattice parameter corresponds to $a = 5.416 \text{ \AA}$. Besides, a difference in the cristalinity depending of the time of reaction can be observed and it is attributed to the formation of 1D nanostructures as reported by *Li et al.*, where it is obtained 1D nanostructures with a preferential growth in the plane (200).

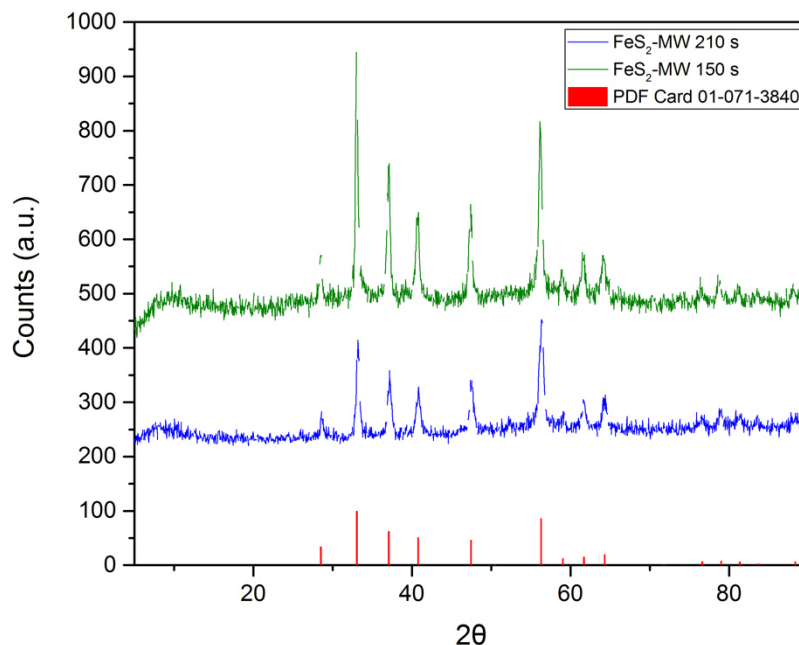


Figure 33. XRD pattern of FeS₂

Figure 34 shows the UV-Vis spectra for FeS₂ at different ratio of Fe²⁺/MPA since it is reported that exists an influence of the ratio of iron source and stabilizer in the morphology obtained. Near 350 and 450 nm are two absorption signals characteristics for

Fe-S systems and around 1100 nm can be observed the tendency of a third absorption peak which it is reported is characteristic of pyrite system. Although, the peak around 1100 nm can only be observed for the experiments 1:4 and 1:3 of $\text{Fe}^{2+}/\text{MPA}$. This phenomena can be explained with PL emission spectra.

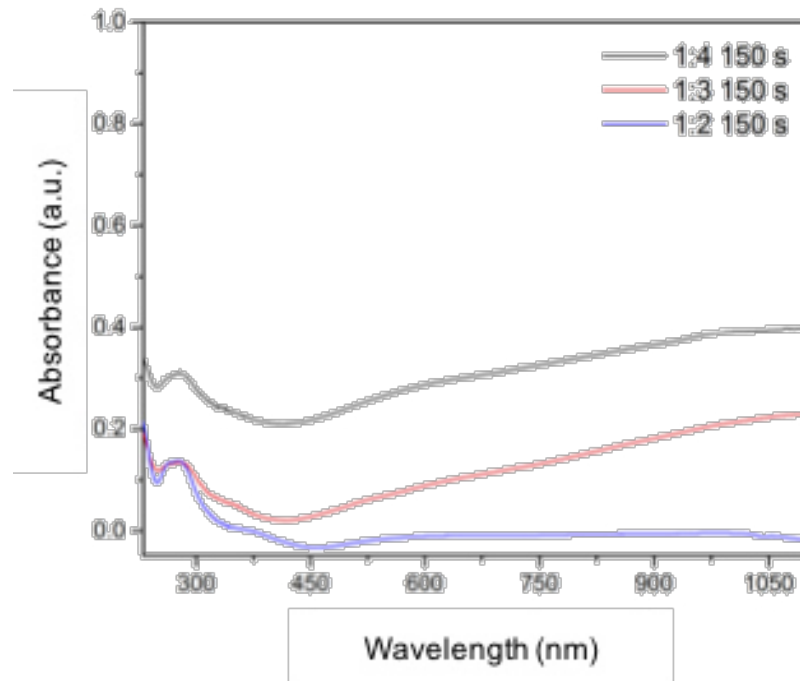


Figure 34. Optical absorption of FeS_2 .

Figure 35 shows the PL emission spectra of FeS_2 where is observed two peaks around 650 nm and 720 nm. The first peak corresponds to Fe-S transitions and it is present in all Fe-S polymorphs since these interactions are equivalent there is not a difference between FeS_2 and others Fe-S compounds. The second peak corresponds to S-S transition since in the crystal lattice of the pyrite, S is tetrahedrally coordinated with 3 atoms of Fe and 1 atom of S, the interactions S-S for pyrite system are stronger than the S-S interactions in the marcasite (FeS_2) system as can be observed for experiment 1:2 where

this peak exhibit a lower intensity. In order to understand the photoluminescence properties of pyrite since the intensity between experiments with ratio 1:4 and 1:3 not correspond to a normal behavior.

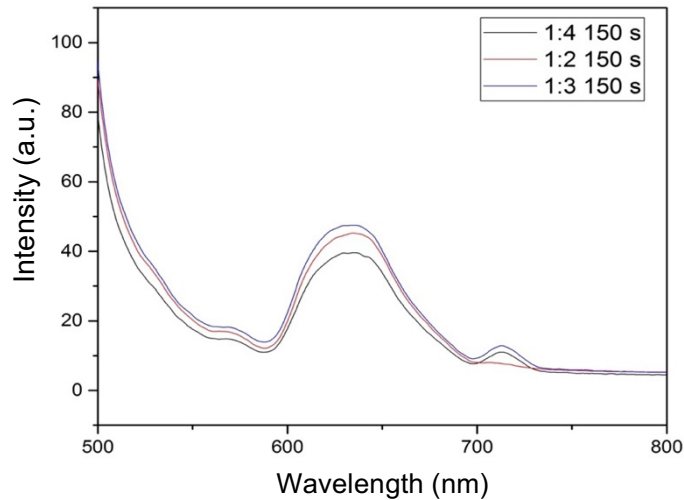


Figure 35. Emission spectra for FeS₂.

It was carried out the structural analysis where in Figure 36, the diffraction pattern for experiments 1:3 and 1:4 exhibit a cubic system without impurities but also, a difference between their intensity due to S-S interactions corresponds to the plane (111) which it is more intense for experiment 1:3 inducing an increasing in its photoluminescence properties. Thus, it can be observed S-S interactions have an effect over optoelectronic properties.

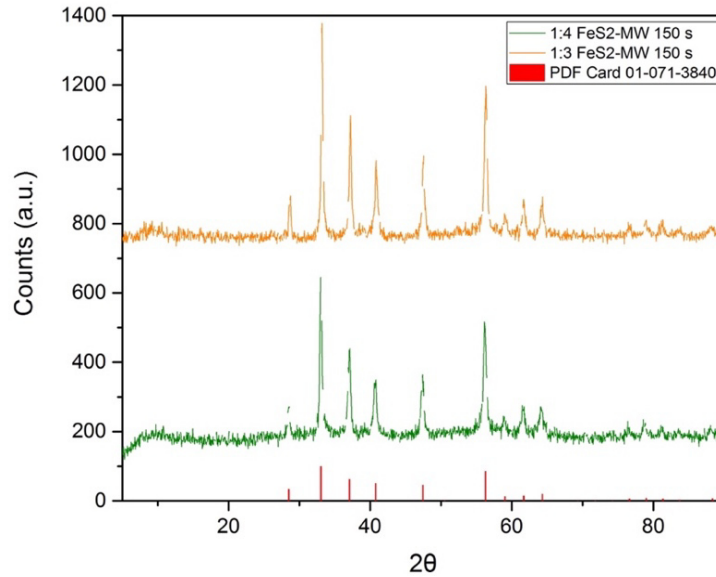


Figure 36. XRD pattern for FeS₂ for experiments 1:4 and 1:3.

Figure 38 shows the SEM (EDS) images for the three experiments of FeS₂ where due to the magnification can not be observed clearly the nanostructures for the semiconductor but it can be seen agglomerates made up of uniform particles with the only composition of Fe-S.

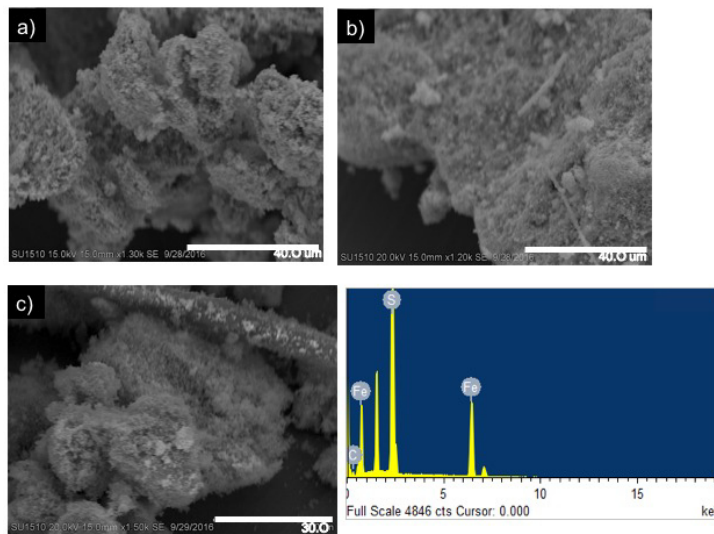


Figure 38. SEM micrography for FeS₂ a) ratio 1:4 b) 1:2, c)1:3 and EDS.

4.4. FeS₂/ZnO

UV-Vis spectrum is given in Figure 39, FeS₂/ZnO exhibits activity in visible region which it is a desirable property for PV application. Also, the absorptions corresponding for ZnO and FeS₂ do not appear instead only appears one single absorption giving the idea the material is working as just one.

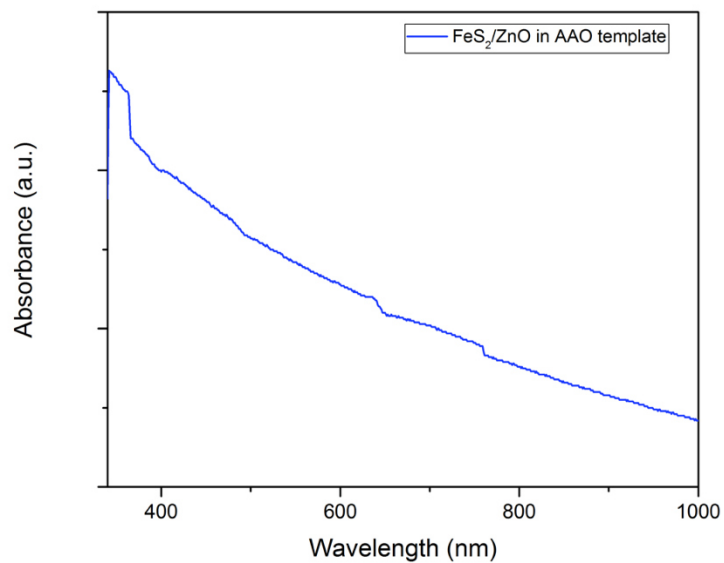


Figure 39. UV-Vis spectrum of FeS₂/ZnO.

PL spectrum is showed in Figure 40, where it can be seen the corresponding transitions of FeS₂ (Fe-S and S-S interactions) and ZnO (Zn-O and O-O), which gives the idea the materials exhibit a coupling but also, exists charge transfer between both systems.

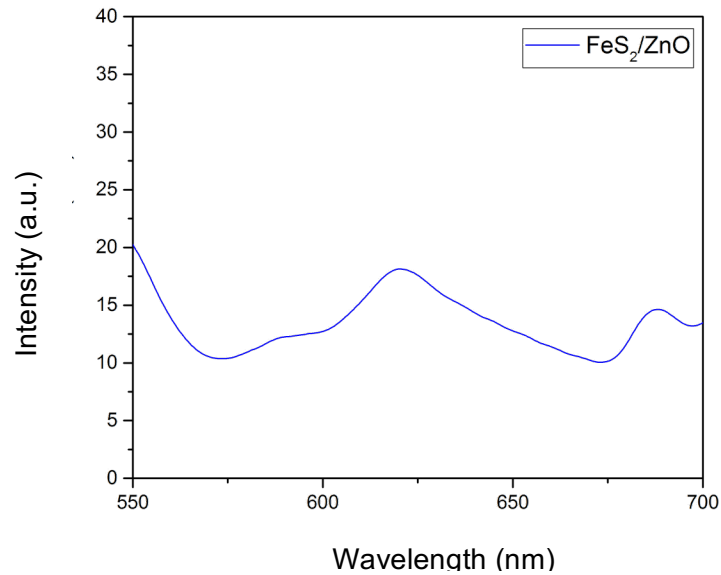


Figure 40. Emission spectrum for FeS₂/ZnO.

Figure 41 shows the SEM micrography corresponding for the core/shell nanowires of FeS₂/ZnO embedded in AAO templates. It can be observed ZnO is incrustated inside the AAO pores but it can not be seen clearly the morphology of the system due to the magnification but according EDS analysis, it can be infered core/shell nanowires are compose of FeS₂ and ZnO.

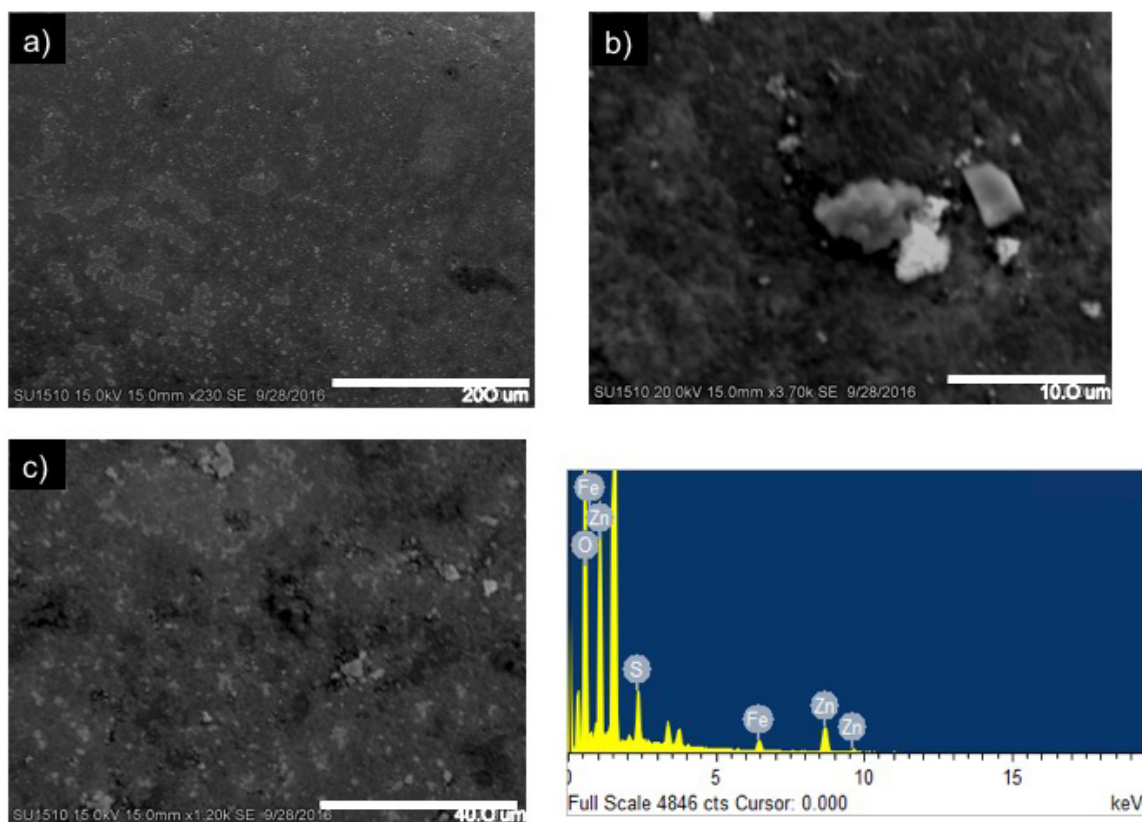


Figure 41. SEM images for FeS₂/ZnO embedded in AAO templates a)X230, b)3.7K and c) 1.2 K and EDS.

4.5. 2,5-Selenophenedicarbaldehyde

In order to corroborate functional groups of the monomer obtained, it was carried out the FT-IR analysis, which is given in Figure 42. It is observed the characteristics vibrations near 898, 1650, 1700 y 2970 cm⁻¹, which correspond to =C-H (hydrogens of the heterocycle), C=O (carbonile), C=C (from heterocycle) y =C-H (also hydrogens from heterocycle) respectively. Also, it is observed for A appears an impurity of diethyl eter due to the presence of characteristic vibrations at 1253, 1394, 2670 y 3452 cm⁻¹, which correspond to C-O, CH₂ y CH₃ respectivamente. Besides around 1650-1700 cm⁻¹ for

experiment B, C=O exhibits a broad peak due to an increase of carbonyl moieties because of disubstitude compound, this effect corroborates the diminish of intensity for =C-H at 2970 cm^{-1} since the bond with H disappear due to it is bonded to aldehyde moiety.

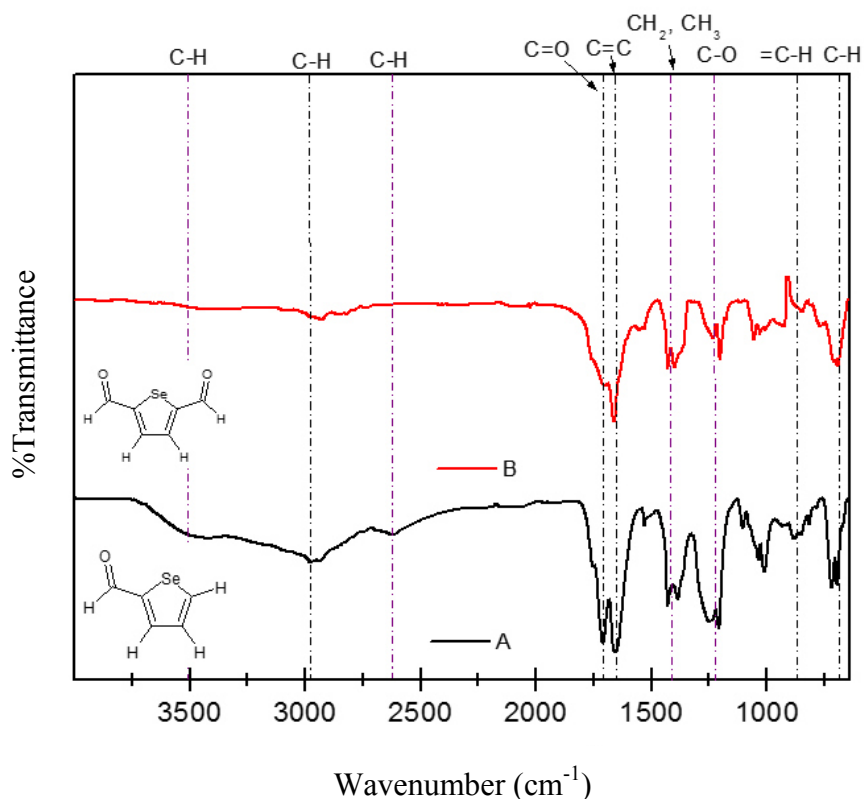


Figure 42. FT-IR spectra for monomer obtained.

Through RMN- ^1H was study the structural characteristics for monomers obtained in order to corroborate the formation of 2,5-Selenophenedicarbaldehyde. The analysis was carried out at 60 Hz in CDCl_3 . RMN- ^1H spectrum corroborates the formation of 2-selenophenedicarbaldehyde, with δ characteristic (chemical shift) at 9.74 ppm (s, 1H), 8.58 ppm (d, 1H), 8.00 ppm (d, 1H), 7.48 ppm (t, 1H) as is shown in Figure 43. For the compound A is observed the formation of 2-selenophenedicarbaldehyde as well due to δ

characteristical (chemical shift) at 9.80 ppm (s, 1H), 8.56 ppm (d, 1H), 8.06 ppm (d, 1H), 7.55 ppm (t, 1H) which are represented in Figure 44. For compound B (Figure 45) is observed δ characteristical of 2,5-Selenophenedicarbaldehyde (chemical shift) at 9.89 ppm (s, 2H), and 8.11 ppm (s, 2H), concluding that for B compound exists a mixture of 2-selenophenedicarbaldehyde /2,5-Selenophenedicarbaldehyde, which the ratio is compared with the integrated area of the peaks, obtaining a ratio of 4:1 of 2-selenophenedicarbaldehyde /2,5-Selenophenedicarbaldehyde, although for C the ratio is 1.2:1 of 2-selenophenedicarbaldehyde /2,5-Selenophenedicarbaldehyde (Figure 46).

According the RMN- H^1 spectra and FT-IR can be concluded that two reactions of Vilsmeier- Haack and an excess of DMF are key conditions for the synthesis of 2,5-Selenophenedicarbaldehyde.

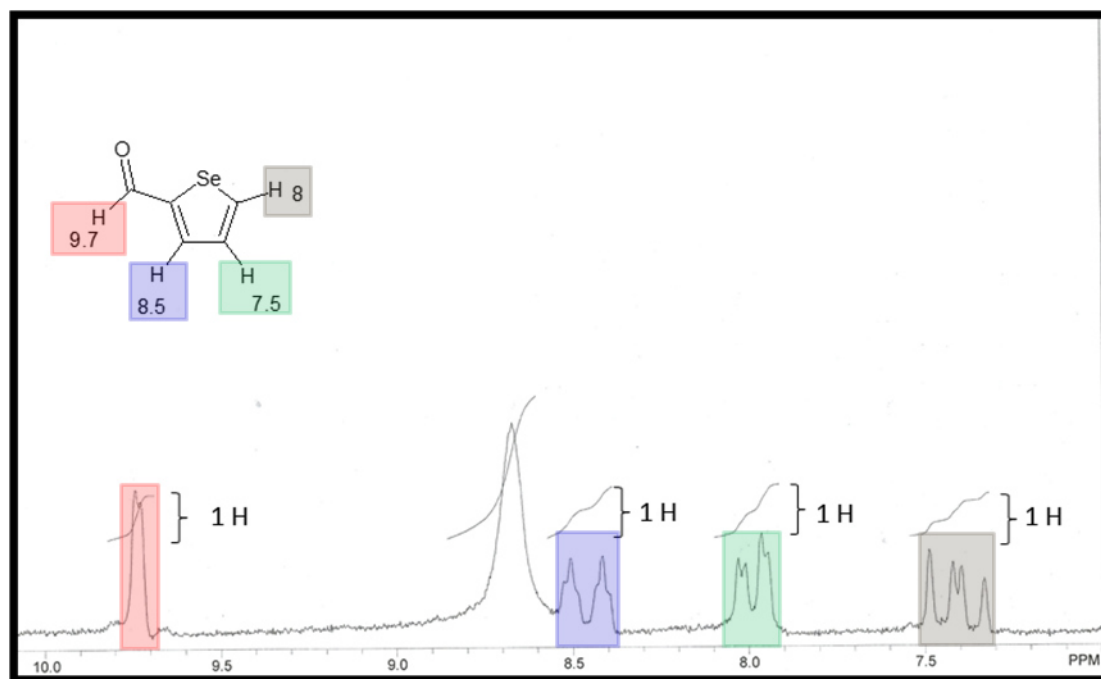


Figure 43. RMN- H^1 spectrum for 2-selenophenedicarbaldehyde.

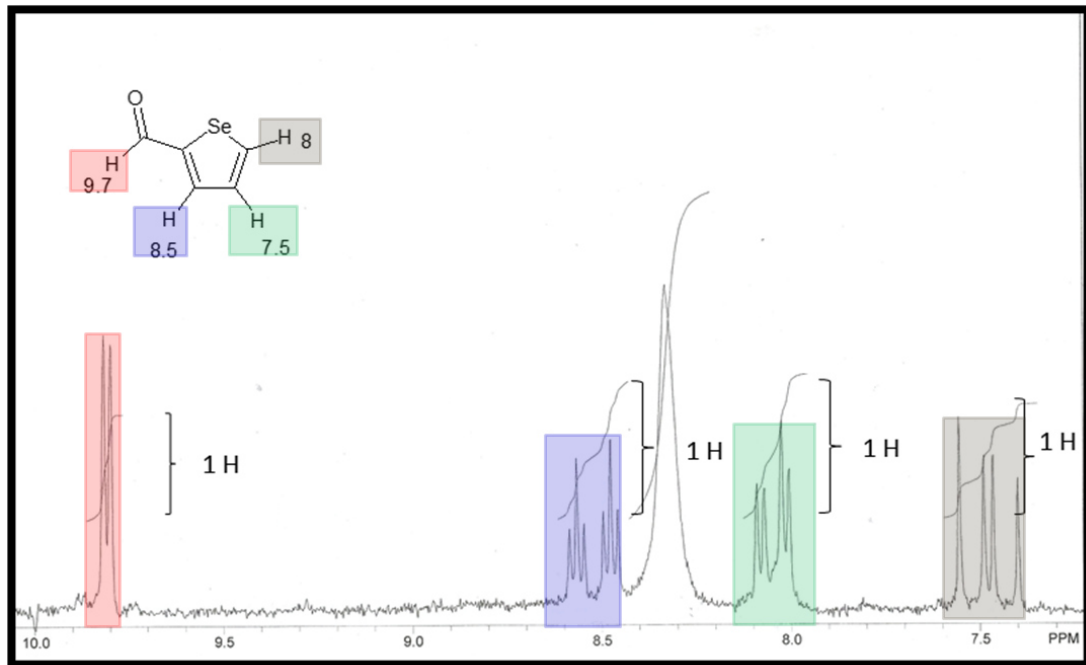


Figure 44. RMN- ^1H spectrum for A.

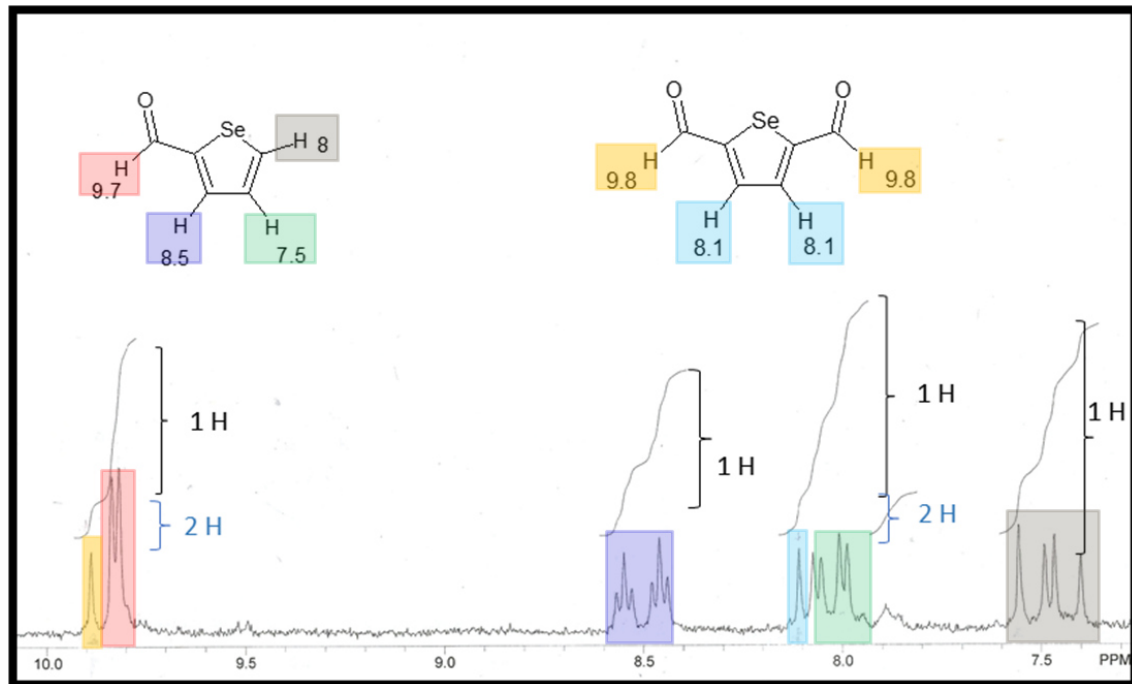


Figure 45. RMN- ^1H spectrum for B.

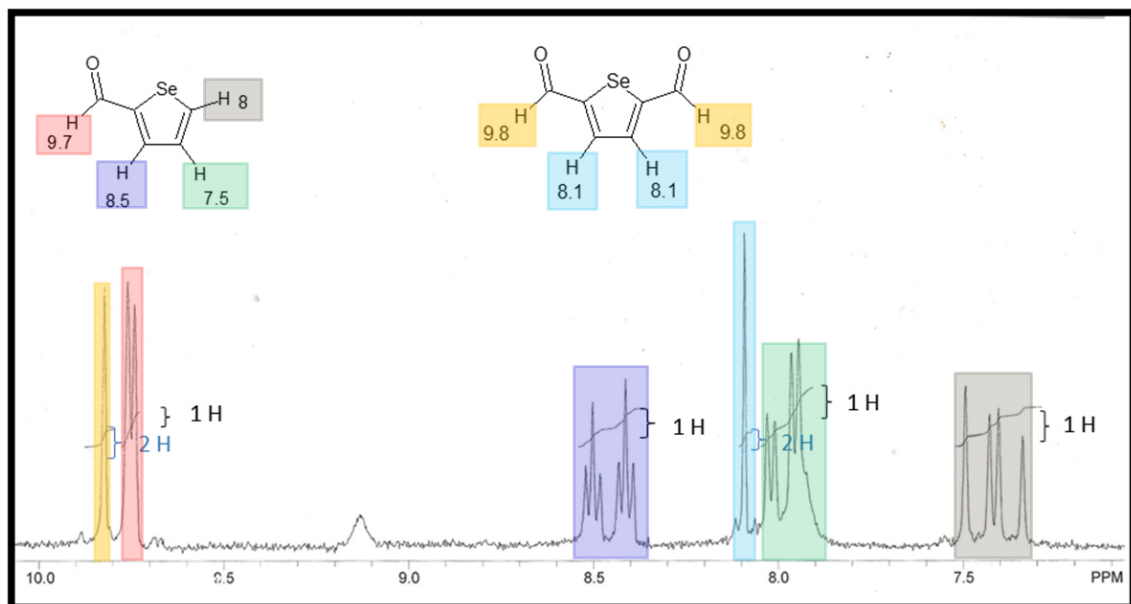


Figure 46. RMN- H^1 spectrum for C.

In order to evaluate the optoelectronic properties of the 2,5-Selenophenedicarbaldehyde was carried out the analysis of absorption and emission spectra. In Figure 47 is showed the optical absorption for the three compounds (A,B, C) which exhibit absorption near 445 nm, 464 nm and 478 nm respectively. The red-shift is attributed to a major content of aldehyde moieties which is due to chromophore nature of aldehyde moieties, which produce a bathochromic effect. This information is corroborated with the behavior observed in RMN- H^1 , where compound A, exhibit an absorption at low wavelength values due to the presence of only a carbonile group. In the other hand B and C, exhibit a major value of wavelength due to presence of double carbonile group.

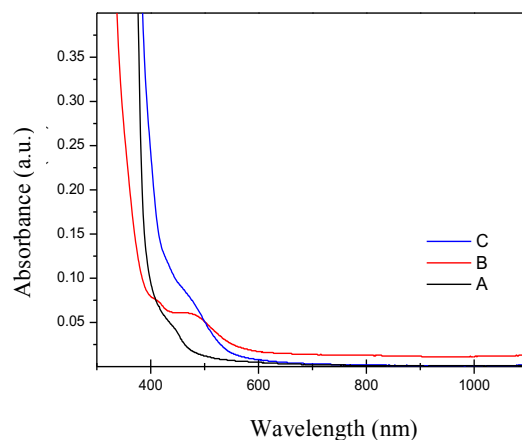


Figure 47. Optical absorption for monomers.

PL spectra is shown in Figure 48. It is observed when compounds are excited at 400 nm the monomers exhibit transitions in around 477, 486 and 525 nm for A, B and C respectively. Which the intensity and emission at major values of wavelength is due to the presence of more aldehyde moieties.

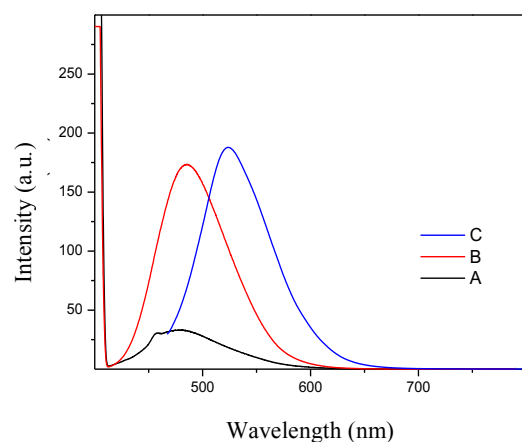


Figure 48. Emission spectra for monomers.

4.6. Polymerization of 2,5-selenofendicarboxaldehyde

In order to corroborate functional groups of the polymer, it was performed a FT-IR analysis. Figure 49 shows the characteristic vibrations near 680-866, 1257, 1462, 1595, 1660 and 2930 cm^{-1} , which correspond to $-\text{CH}=\text{CH}-$ (aromatic, hydrogen heterocycle), $\text{C}=\text{O}$ (carbonile), $-\text{CH}-$ (two peaks for aromatics), $\text{C}=\text{O}$ (carbonile) and $-\text{C}=\text{C}-$ (conjugated backbone) respectively. Also, it is observed the presence of peaks around 1031 and 3327 cm^{-1} , which are characteristic of $-\text{C}-\text{OH}$ y $-\text{OH}$ present in water and ethanol impurities of the purity process.

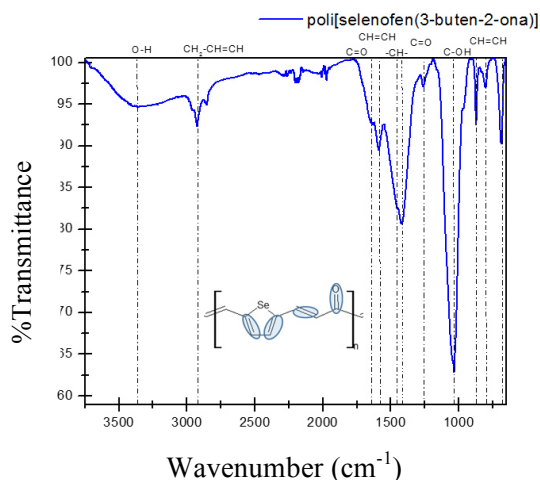


Figure 49. FT-IR spectrum for conducting polymer.

Optoelectronic properties were evaluated by UV-Vis and PL analysis. Figure 50 shows the optical absorption at 510 nm with an approximated $E_g = 2.4$ eV, indicating activity in the visible range, which is important for PV application. Although, the E_g value is higher compared to values reported for conducting polymers (1.6-2.3 eV).

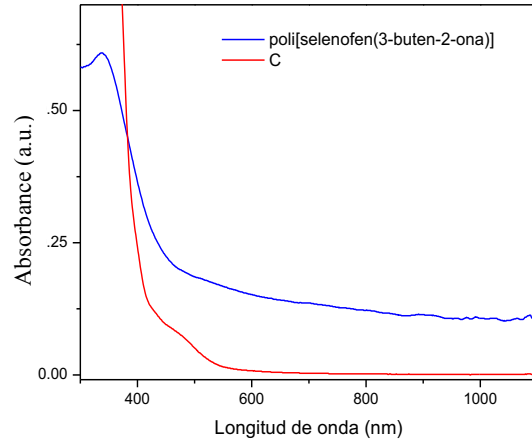


Figure 50. UV-Vis spectra for monomer and polyselenophene.

PL spectrum is shown in Figure 51 where it is observed the emission spectrum and four peaks at 330, 564, 612 and 642 nm. The first one corresponds to the $\pi-\pi^*$ transition, which it is characteristic of conducting polymer while the signals around 564, 612 and 642 nm are attributed to interchain transfer and the π -stacking. The interchain transfer refers to the charge transport between the backbones of the conjugated polymers while, π -stacking consists in the charge transport between π orbitals which are overlapped in Y direction.

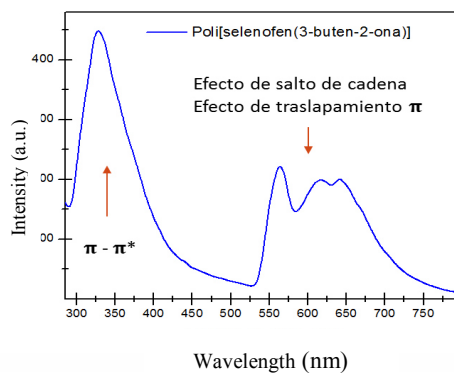


Figure 51. PL spectrum of a polyselenophene.

Chapter 5

Conclusions

5.1. Preliminary conclusions

- AAO templates were obtained by two-step anodization. The AAO templates exhibit diameter of pores about 50 nm.
- ZnO nanotubes were obtained by immersion method of AAO templates.
- The optical analysis of ZnO exhibit an absorption signal around 390 nm and an estimated of $E_g = 3.18$ eV.
- Through PL, ZnO exhibit common transitions for 1D systems which, correspond to O vacant to O interstitial and Zn to O interaction.
- FeS₂ (pyrite) was obtained by microwave heating method.
- Structural analysis revealed, crystal lattice of FeS₂ corresponds to cubic structure with lattice constant of $a = 5.41$ Å. Any impurities of troilite or marcasite appeared.
- FeS₂ (pyrite) exhibit absorption around 350 nm and 1100 nm, the first signal according the transition present in all Fe-S systems and the second one corresponds to a characteristic transition of FeS₂.
- Through PL, interactions of Fe-S and S-S are revealed. Also, it is observed a relation between the crystal lattice of FeS₂ and its optoelectronic properties, which increment or diminish depending of how strong S-S intereactions are.
- According to SEM (EDS), FeS₂ exhibit a uniform morphology and also, it only consists of Fe and S indicating the samples do not have the presence of iron oxides.

- Core/shell nanowires of FeS₂/ZnO were obtained by AAO templates assisted method.
- Core/shell nanowires of FeS₂/ZnO exhibit coupling and charge transference according the optical analysis.
- FeS₂/ZnO exhibit absorption in the visible range and transitions corresponding to both materials.
- The derivative of polyselenophene exhibit absorption in the visible range but also, charge transfer due to π - π^* transitions and the π -stacking.

Chapter 6

References

- [1] U.S. Energy Information Administration (EIA). [online] Available at: <https://www.eia.gov> [Accessed 27 Oct. 2015].
- [2] Chu, Y. (2011) ‘Review and Comparison of Different Solar Energy Technologies’, Global Energy Network Institute, (August).
- [3] Secretaría de energía (SENER). [online] Available at: <http://www.gob.mx/sener> [Accessed 27 Oct. 2015].
- [4] PEMEX | Transformación para impulsar a México. [online] Available at: <http://www.pemex.com/> [Accessed 27 Oct. 2015].
- [5] Mundo-Hernández, J., De Celis Alonso, B., Hernández-Álvarez, J. and De Celis-Carrillo, B. (2014) ‘An overview of solar photovoltaic energy in Mexico and Germany’, *Renew. Sust. Energ. Rev.*, 31(1), pp. 639–649. doi: 10.1016/j.rser.2013.12.029.
- [6] Solargis.com. Accurate and efficient solar energy assessment | Solargis. [online] Available at: <http://solargis.com> [Accessed 30 Oct. 2015].
- [7] Alemán-Nava, G. S., Casiano-Flores, V. H., Cárdenas-Chávez, D. L., Díaz-Chavez, R., Scarlat, N., Mahlkecht, J., Dallemand, J. F. and Parra, R. (2014) ‘Renewable energy research progress in Mexico: A review’, *Renew. Sust. Energ. Rev.*, 32(1), pp. 140–153. doi: 10.1016/j.rser.2014.01.004.
- [8] Zhang, Q., Uchaker, E., Candelaria, S. and Cao, G. (2012) ‘Nanomaterials for energy conversion and storage’, *Chem. Soc. Rev.*, 42(7), pp. 3127–3171. doi: 10.1155/2012/159249.
- [9] Chen, G., Seo, J., Yang, C. and Prasad, P. N. (2013) ‘Nanochemistry and nanomaterials for photovoltaics.’, *Chem.Soc. Rev.*, 42(21), pp. 8304–38. doi: 10.1039/c3cs60054h.

- [10] Ramsden, J. J. (2014) What is Nanotechnology? In: Ramsden, J. J. *Applied Nanotechnology The Conversion of Research Results to Products (Micro and Nano Technologies)*. U.S.A., Elsevier, p. 3-12.
- [11] Loss, M. (2015) Nanoscience and Nanotechnology. In: Loss, M. *Carbon nanotube reinforced composites*. U.S.A., Elsevier, p. 1-36.
- [12] Miller, J. C., Serrato, R., Represas-Cardenas J.M. and Kundahl G. (2005) Introduction to Nanotechnology. In: Miller, J. C., Serrato, R., Represas-Cardenas J.M. and Kundahl G. *The handbook of nanotechnology. Business, Policy, and Intellectual Property Law*. U.S.A., John Wiley & Sons. p.13-31.
- [13] Ashby, M.F., Ferreira, P.J. and Schodek, D.L. (2007) Nanomaterials: Classes and Fundamentals. In: Ashby, M.F., Ferreira, P.J. and Schodek, D.L. *Nanomaterials, nanotechnologies and design*. U.S.A., Elsevier, p. 177-197.
- [14] Kittel, C. (2005) Energy bands. In: Kittel, C. *Introduction to solid state physics*. U.S.A., John Wiley & Sons, p. 1228-1266.
- [15] Tipler, P., Mosca, G. (2010) Solids. In: Tipler, P. *Physics for Scientists and Engineers*. U.S.A., W. H. Freeman & Company, p. 161-182.
- [16] Gupta, K. M. and Gupta, N. (2015) Semiconductor Materials: Their Properties, Applications, and Recent Advances. In: Gupta, K. M. and Gupta, N. *Advanced semiconducting materials and devices*. U.S.A., Springer, p. 3-40.
- [17] Huebener, R. P. (2015) Less Can Be More: Semiconductors. In: Huebener, R.P. *Conductors , Semiconductors, Superconductors*. Switzerland, Springer International, p. 73-96.

- [18] Jacoboni, C. (2010). Semiconductors. In: Jacoboni, C. *Theory of Electron Transport in Semiconductors*. Berlin, Springer, p. 103-123.
- [19] Yu, P.Y. and Cardona, M. (2010) Introduction. In: Yu, P.Y. and Cardona, M. *Fundamentals of Semiconductors Physics and Materials Properties*. Berlin, Springer, p. 2-14.
- [20] Ragoussi, M.-E. and Torres, T. S. (2015) ‘New generation solar cells: concepts, trends and perspectives’, *Chem. Commun.*, 51(19), pp. 3957–3972. doi: 10.1039/c4cc09888a.
- [21] Babu, V. J., Vempati, S., Sundarrajan, S., Sireesha, M. and Ramakrishna, S. (2014) ‘Effective nanostructured morphologies for efficient hybrid solar cells’, *Sol. Energy*, 106(1), pp. 1–22. doi: 10.1016/j.solener.2013.08.037.
- [22] Parida, B., Iniyar, S. and Goic, R. (2011) ‘A review of solar photovoltaic technologies’, *Renew. Sust. Energ. Rev.*, 15(3), pp. 1625–1636. doi: 10.1016/j.rser.2010.11.032.
- [23] Asim, N., Sopian, K., Ahmadi, S., Saeedfar, K., Alghoul, M. A., Saadatian, O. and Zaidi, S. H. (2012) ‘A review on the role of materials science in solar cells’, *Renew. Sust. Energ. Rev.*, 16(8), pp. 5834–5847. doi: 10.1016/j.rser.2012.06.004.
- [24] Green, M. A. (2002) ‘Photovoltaic principles’, *Physica E*, 14(1–2), pp. 11–17. doi: 10.1016/S1386-9477(02)00354-5.
- [25] Chandrasekaran, J., Nithyaprakash, D., Ajjan, K. B., Maruthamuthu, S., Manoharan, D. and Kumar, S. (2011) ‘Hybrid solar cell based on blending of organic and inorganic materials - An overview’, *Renew. Sust. Energ. Rev.*, 15(2), pp. 1228–1238. doi: 10.1016/j.rser.2010.09.017.

- [26] Arici, E. and Sariciftci, N. S. (2008) Hybrid solar cells. In: **Nalwa, H.S. *Encyclopedia of Nanoscience and Nanotechnology***. U.S.A., Journal of Nanoscience and Nanotechnology, p. 581–588.
- [27] Reiss, P., Couderc, E., De Girolamo, J. and Pron, A. (2011) ‘Conjugated polymers/semiconductor nanocrystals hybrid materials--preparation, electrical transport properties and applications.’, *Nanoscale*, 3(2), pp. 446–89. doi: 10.1039/c0nr00403k.
- [28] Wright, M. and Uddin, A. (2012) ‘Organic-inorganic hybrid solar cells: A comparative review’, *Sol. Energ. Mat. Sol. Cells*, 107(1), pp. 87–111. doi: 10.1016/j.solmat.2012.07.006.
- [29] Liu, R. (2014) ‘Hybrid organic/inorganic nanocomposites for photovoltaic cells’, *Materials*, 7(4), pp. 2747–2771. doi: 10.3390/ma7042747.
- [30] Fan, X., Zhang, M., Wang, X., Yang, F. and Meng, X. (2013) ‘Recent progress in organic–inorganic hybrid solar cells’, *J. Mater. Chem. A*, 1(31), pp. 8694–8709. doi: 10.1039/c3ta11200d.
- [31] Xu, T. and Qiao, Q. (2011) ‘Conjugated polymer–inorganic semiconductor hybrid solar cells’, *Energy Environ. Sci.*, 4(8), p. 2700. doi: 10.1039/c0ee00632g.
- [32] Balazs, D.M., Speirs, M. J. and Loi, M. A. (2014) Colloidal Inorganic–Organic Hybrid Solar Cells. In: Huang, J and Huand, H. *Organic and Hybrid Solar Cells*. Switzerland, Springer International, p. 301-337.
- [33] Janssen, R. a J., Hummelen, J. C. and Sariciftci, N. S. (2005) ‘Polymer-Fullerene Bulk Heterojunction Solar Cells’, *MRS Bulletin*, pp. 1–68. doi: 10.1088/0034-4885/73/9/096401

- [34] Sun, H., Deng, J., Qiu, L., Fang, X. and Peng, H. (2015) ‘Recent progress in solar cells based on one-dimensional nanomaterials’, *Energy Environ. Sci.*, 8(4), pp. 1139–1159. doi: 10.1039/C4EE03853C.
- [35] Xia, Y., Yang, P., Sun, Y., Wu, Y., Mayers, B., Gates, B., Yin, Y., Kim, F. and Yan, H. (2003) ‘One-Dimensional Nanostructures : Synthesis , Characterization , and Applications **’, *Adv. Mater.*, 15(5), pp. 353–389. doi: 0935-9648/03/0503-0353.
- [36] Al-Kaysi, R. O., Ghaddar, T. H. and Guirado, G. (2009) ‘Fabrication of one-dimensional organic nanostructures using anodic aluminum oxide templates’, *Journal of Nanomaterials*, 2009 (2009), pp. 1–14. doi: 10.1155/2009/436375.
- [37] Huczko, A. (2000) ‘Template-based synthesis of nanomaterials’, *Appl. Phys. A*, 70(4), pp. 365–376. doi: 10.1007/s003390051050.
- [38] Lai, M. and Riley, D. J. (2008) ‘Templated electrosynthesis of nanomaterials and porous structures’, *J. Colloid Interface Sci.*, 323(2), pp. 203–212. doi: 10.1016/j.jcis.2008.04.054.
- [39] Cao, G. and Liu, D. (2008) ‘Template-based synthesis of nanorod , nanowire , and nanotube arrays’, *Adv. Colloid Interface Sci.*, 136(1-2), pp. 45–64. doi: 10.1016/j.cis.2007.07.003.
- [40] Lee, W. and Park, S.-J. S. S. (2014) ‘Porous anodic aluminum oxide: anodization and templated synthesis of functional nanostructures’, *Chem. Rev.*, 114(15), pp. 7487–7556. doi: 10.1021/cr500002z.
- [41] Şişman, İ. (2011) Template-Assisted Electrochemical Synthesis of Semiconductor Nanowires. In: Hashim, A. *Nanowires - Implementations and Applications*. China, InTech, p.41-58.

- [42] Sverdlin, Alexey (2003) Introduction to Aluminum. In: Totten, G.E. and MacKenzie, D.S. *Handbook of Aluminum*. U.S.A., Marcel Dekker, p. 1-32.
- [43] Md Jani, A. M., Losic, D. and Voelcker, N. H. (2013) ‘Nanoporous anodic aluminium oxide: Advances in surface engineering and emerging applications’, *Prog. Mater Sci.*, 58(5), pp. 636–704. doi: 10.1016/j.pmatsci.2013.01.002.
- [44] Zhang, J., Kielbasa, J. E. and Carroll, D. L. (2010) ‘Controllable fabrication of porous alumina templates for nanostructures synthesis’, *Mater. Chem. Phys.*, 122(1), pp. 295–300. doi: 10.1016/j.matchemphys.2010.02.023.
- [45] Samantilleke, a. P., Carneiro, J. O., Azevedo, S., Thuy, T. and Teixeira, V. (2013) ‘Electrochemical Anodizing, Structural and Mechanical Characterization of Nanoporous Alumina Templates’, *Journal of Nano Research*, 25(1), pp. 77–89. doi: 10.4028/www.scientific.net/JNanoR.25.77.
- [46] Michalska-Domańska, M., Norek, M., Stępniewski, W. J. and Budner, B. (2013) ‘Fabrication of high quality anodic aluminum oxide (AAO) on low purity aluminum - A comparative study with the AAO produced on high purity aluminum’, *Electrochim. Acta*, 105(1), pp. 424–432. doi: 10.1016/j.electacta.2013.04.160.
- [47] Liu, S., Xiong, Z., Zhu, C., Li, M., Zheng, M. and Shen, W. (2014) ‘Fast anodization fabrication of AAO and barrier perforation process on ITO glass.’, *Nanoscale Res. Lett.*, 9(159), p. 1–8. doi: 10.1186/1556-276X-9-159.
- [48] Cui, J., Wu, Y., Wang, Y., Zheng, H., Xu, G. and Zhang, X. (2012) ‘In-situ fabrication of AAO template without oxide barrier layer and its applications.’, *J. Nanosci. Nanotechnol.*, 12(4), pp. 3130–3134. doi: 10.1166/jnn.2012.5835.

- [49] Santos, A., Kumeria, T. and Losic, D. (2014) ‘Nanoporous anodic alumina: A versatile platform for optical biosensors’, *Materials*, 7(6), pp. 4297–4320. doi: 10.3390/ma7064297.
- [50] Wen, L., Wang, Z., Mi, Y., Xu, R., Yu, S. H. and Lei, Y. (2015) ‘Designing Heterogeneous 1D Nanostructure Arrays Based on AAO Templates for Energy Applications’, *Small*, 11(28), pp. 3408–3428. doi: 10.1002/sml.201500120.
- [51] Masuda, H. and Fukuda, K. (1995) ‘Ordered Metal Nanohole Arrays Made by a Two-Step Replication of Honeycomb Structures of Anodic Alumina’, *Science*, 268(5216), pp. 1466–1468. doi: 10.1126/science.268.5216.1466.
- [52] Stępniewski, W. J. and Salerno, M. (2014) Fabrication of nanowires and nanotubes by anodic alumina template-assisted electrodeposition. In: Ahmed, W and Ali, N. *Manufacturing nanostructures*. U.S.A., One Central Press, pp. 321–357.
- [53] Su, B. Z. and Zhou, W. (2008) ‘Formation Mechanism of Porous Anodic Aluminium and Titanium Oxides **’, *Adv. Mater.*, pp. 3663–3667. doi: 10.1002/adma.200800845.
- [54] Poinern, G. E. J., Ali, N. and Fawcett, D. (2010) ‘Progress in nano-engineered anodic aluminum oxide membrane development’, *Materials*. 4(3), pp. 487-526. doi: 10.3390/ma4030487.
- [55] Wadia, C., Alivisatos, A. P. and Kammen, D. M. (2009) ‘Materials Availability Expands the Opportunity for Large-Scale Photovoltaics Deployment’, *Environ. Sci. Technol.*, 43(6), pp. 2072–2077. doi: 10.1021/es8019534.
- [56] Cabán-Acevedo, M., Faber, M. S., Tan, Y., Hamers, R. J. and Jin, S. (2012) ‘Synthesis and properties of semiconducting iron pyrite (FeS₂) nanowires’, *Nano Lett.*, 12(4), pp. 1977–1982. doi: 10.1021/nl2045364.

- [57] Yakovkin, I. N. and Petrova, N. V (2016) ‘Applied Surface Science Influence of the thickness and surface composition on the electronic structure of FeS₂ layers’, *Appl. Surf. Sci.*, 377(1), pp. 184–190. doi: 10.1016/j.apsusc.2016.03.188.
- [58] Wang, M. D., Xing, C. C., Cao, K., Zhang, L., Liu, J. B. and Meng, L. (2014) ‘Template-directed synthesis of pyrite (FeS₂) nanorod arrays with an enhanced photoresponse’, *J. Mater. Chem. A*, 2(25), pp. 9496–9505. doi: 10.1039/c4ta00759j.
- [59] Wu, J., Liu, L., Liu, S., Yu, P., Zheng, Z., Shafa, M., Zhou, Z., Li, H., Ji, H. and Wang, Z. M. (2014) ‘High responsivity photoconductors based on iron pyrite nanowires using sulfurization of anodized iron oxide nanotubes’, *Nano Lett.*, 14(10), pp. 6002–6009. doi: 10.1021/nl503059t.
- [60] Wan, D., Wang, Y., Zhou, Z., Yang, G., Wang, B. and Wei, L. (2005) ‘Fabrication of the ordered FeS₂ (pyrite) nanowire arrays in anodic aluminum oxide’, *Mat. Sci. Eng. B-Solid*, 122(2), pp. 156–159. doi: 10.1016/j.mseb.2005.05.003.
- [61] Xian, H., Zhu, J., Liang, X. and He, H. (2016) ‘Morphology controllable syntheses of micro- and nano-iron pyrite mono- and poly-crystals: a review’, *RSC Adv.*, 6(38), pp. 31988–31999. doi: 10.1039/C6RA04874A.
- [62] Wadia, C., Wu, Y., Gul, S. and Alivisatos, A. P. (2009) ‘Surfactant-Assisted Hydrothermal Synthesis of Single phase Pyrite FeS₂ Nanocrystals’, *Chem. Mater.*, 13(4), pp. 2568–2570. doi: 10.1021/cm901273v.
- [63] Beek, W. J. E., Janssen, R. and Wienk, M. (2004) ‘Efficient Hybrid Solar Cells from Zinc Oxide Nanoparticles and a Conjugated Polymer’, *Adv. Mater.*, 16(12), pp. 1009–1013. doi: 10.1002/adma.200306659.

- [64] Sahu, D. R., Liu, C. P., Wang, R. C., Kuo, C. L. and Huang, J. L. (2013) ‘Growth and application of ZnO nanostructures’, *Int. J. Appl. Ceram. Technol.*, 10(5), pp. 814–838. doi: 10.1111/j.1744-7402.2012.02795.x.
- [65] Cauda, V., Gazia, R., Porro, S., Stassi, S., Canavese, G., Roppolo, I. and Chiolerio, A. (2014). Nanostructured ZnO Materials: Synthesis, Properties and Applications. In: Bhushan, B., Luo, D., Schricker, S.R., Sigmund, W. and Zauscher, S. *Handbook of Nanomaterials Properties*. Berlin, Springer, p. 137-177.
- [66] Chou, T. P., Zhang, Q., Fryxell, G. E. and Cao, G. (2007) ‘Hierarchically structured ZnO film for dye-sensitized solar cells with enhanced energy conversion efficiency’, *Adv. Mater.*, 19(18), pp. 2588–2592. doi: 10.1002/adma.200602927.
- [67] Xu, S. and Wang, Z. L. (2011) ‘One-dimensional ZnO nanostructures: Solution growth and functional properties’, *Nano Res.*, 4(11), pp. 1013–1098. doi: 10.1007/s12274-011-0160-7.
- [68] Djurišić, A. B. and Leung, Y. H. (2006) ‘Optical properties of ZnO nanostructures’, *Small*, 2(8–9), pp. 944–961. doi: 10.1002/sml.200600134.
- [69] Kashif, M, Akhtar, M.N., Nasir, N. and Yahya, N. (2010) Versatility of ZnO Nanostructures. In: Yahya. N. *Carbon and Oxide Nanostructure*. Berlin, Springer, p. 219-244.
- [70] Wan, M. (2008) Introduction of Conducting Polymers. In: Wan, M. *Conducting Polymers with Micro or Nanometer Structure*. Berlin, Springer, p. 1-13.
- [71] Kline, R. J. and McGehee, M. D. (2006) ‘Morphology and Charge Transport in Conjugated Polymers’, *J. Macromol. Sci. Polymer Rev.*, 46(1), pp. 27–45. doi: 10.1080/15321790500471194.

- [72] Hoppe, H and Sariciftci, N.S. (2008) Polymer Solar Cells. In: Marder, S.R. and Lee, K.S. *Photoresponsive Polymers II*. Berlin, Springer Heidelberg, p. 1-86.
- [73] Bagheri, H., Ayazi, Z. and Naderi, M. (2013) ‘Conductive polymer-based microextraction methods: A review’, *Anal. Chim. Acta*, 767(1), pp. 1–13. doi: 10.1016/j.aca.2012.12.013.
- [74] Balint, R., Cassidy, N. J. and Cartmell, S. H. (2014) ‘Conductive polymers: Towards a smart biomaterial for tissue engineering’, *Acta Biomater.*, 10(6), pp. 2341–2353. doi: 10.1016/j.actbio.2014.02.015.
- [75] Dai, L. (2004) Conducting Polymers. In: Dai, L. *Intelligent Macromolecules for Smart Devices*. London, Springer-Verlag, p. 41-80.
- [76] Jang, J. (2006). Generic Synthesis of Conducting Polymers. In: Lee, K.S. *Conducting Polymer Nanomaterials and Their Applications*. Berlin, Springer-Verlag, p- 195-198.
- [77] Otero, T. F. (2003) ‘Polimeros Conductores: Sintesis, Propiedades Y Aplicaciones Electroquimicas’, *Revista Iberoamericana de Polímeros*, 4(4), pp. 1–32. doi: n/a.
- [78] Bundgaard, E. and Krebs, F. C. (2007) ‘Low band gap polymers for organic photovoltaics’, *Sol. Energ. Mat. Sol. Cells*, 91(11), pp. 954–985. doi: 10.1016/j.solmat.2007.01.015.
- [79] Helgesen, M., Sondergaard, R. and Krebs, F. C. (2010) ‘Advanced materials and processes for polymer solar cell devices’, *J. Mater. Chem.*, 20(1), pp. 36–60. doi: 10.1039/b913168j.
- [80] Bhattacharyya, D. and Gleason, K. (2011) ‘Low Band Gap Conformal Polyselenophene Thin Films by Oxidative Chemical Vapor Deposition’, *J. Mater. Chem.*, 22(2), pp. 405–410. doi: 10.1039/c1jm13755g

- [81] Patra, A. and Bendikov, M. (2009) ‘Polyselenophenes’, *J. Mater. Chem.*, 20(3), pp. 422–433. doi: 10.1039/b908983g.
- [82] Das, S. and Zade, S. (2010) ‘Poly(cyclopenta[c]selenophene): A New Polyselenophene’, *Chem. Commun.*, 46(7), pp. 1168–1170. doi: 10.1039/b915826j.
- [83] Poverenov, E., Sheynin, Y., Zamoshchik, N., Patra, A., Leitus, G.; Perepichka, I. and Bendikov, M. (2012) ‘Flat Conjugated Polymers Combining a Relatively Low HOMO Energy Level and Band Gap: Polyselenophenes versus Polythiophenes’, *J. Mater. Chem.*, 22(29), pp. 14645–14655. doi: 10.1039/c2jm31035j.
- [84] Heeney, M., Zhang, W., Crouch, D., Chabinyo, M., Gordeyev, S., Hamilton, R., Higgins, S., McCulloch, I., Skabara, P., Sparrowe, D.; *et al.* (2007) ‘Regioregular poly(3-Hexyl)selenophene: A Low Band Gap Organic Hole Transporting Polymer’, *Chem. Commun.*, 0(47), pp. 506–5063. doi: 10.1039/b712398a.
- [85] Greenham N., Peng X and Alivisatos A. (1996) ‘Charge separation and transport in conjugated-polymer/semiconductor-nanocrystal composites studied by photoluminescence quenching and photoconductivity’, *Phys. Rev. B.*, 54(24), pp. 17628–17637. doi: 10.1103/PhysRevB.54.17628.
- [86] Zhang, S., Peng, S., Liu, S., Ren, L., Wang, S. and Fu, J. (2013) ‘Preparation of Polyaniline-Coated B-AgVO₃ Nanowires and Their Application in Lithium-Ion Battery’, *Mater. Lett.*, 110(1), pp. 168–171. doi: 10.1016/j.matlet.2013.08.029.
- [87] Xia, X., Chao, D., Fan, Z., Guan, C., Cao, X., Zhang, H. and Fan, H. (2014) ‘A New Type of Porous Graphite Foams and Their Integrated Composites with Oxide/Polymer Core/Shell Nanowires for Supercapacitors: Structural Design, Fabrication, and Full

Supercapacitor Demonstrations’, *Nano Lett.*, 14(3), pp. 1651–1658. doi: 10.1021/nl5001778.

[88] Tripathi, B. and Shahi, V. (2011) ‘Organic–inorganic Nanocomposite Polymer Electrolyte Membranes for Fuel Cell Applications’, *Prog. Polym. Sci.*, 36(7), pp. 945–979. doi: 10.1016/j.jiec.2014.04.030.

[89] Su, S., Wang, Y., Wang, J., Xu, Z. and Chen, J. (2014) ‘Material optimum choices and parametric design strategies of a photon-enhanced solar cell hybrid system’, *Sol. Energ. Mat. Sol. Cells*, 128(1), pp. 112–118. doi: 10.1016/j.solmat.2014.04.038.

[90] Li, S.S. and Chen, C.W. (2013) ‘Polymer –metal- oxide hybrid solar cells’, *J. Mater. Chem. A.*, 1(36), pp. 10574–10591. doi: 10.1039/c3ta11998j.

[91] Johansson, J. and Dick, K. (2011) ‘Recent Advances in Semiconductor Nanowire Heterostructures’, *Cryst. Eng. Comm.*, 13(24), pp. 7175–7184. doi: 10.1039/c1ce05821e.

[92] Tian, B., Kempa, T. and Lieber, C. (2009) ‘Single nanowire photovoltaics’, *Chem. Soc. Rev.*, 38(1), pp. 16–24. doi: 10.1039/b718703n.

[93] Rabin, O., Black, M.R., Kong, J. and Dresselhaus, G. (2010) Nanowires. In: Bhushan, B. *Handbook of Nanotechnology*. Berlin, Springer Heidelberg, p. 99-138.

[94] Liu, Y., Hou, D. and Wang, G. (2003) ‘Synthesis and Characterization of SnS Nanowires in Cetyltrimethylammoniumbromide (CTAB) Aqueous Solution’, *Chem. Phys. Lett.* 379(1-2), pp. 67–73. doi:10.1016/j.cplett.2003.08.014.

[95] Mondal, S., Dhar, A. and Ray, S. (2007) ‘Optical Properties of CdS Nanowires Prepared by DC Electrochemical Deposition in Porous Alumina Template’, *Mater. Sci. Semicond. Process.*, 10(4-5), pp. 185–193. doi: 10.1016/j.mssp.2007.11.003.

- [96] Yang, P., Yan, H., Mao, S., Russo, R., Johnson, J., Saykally, R., Morris, N., Pham, J., He, R. and Choi, H.J. (2002) 'Controlled Growth of ZnO Nanowires and Their Optical Properties', *Adv. Funct. Mater.*, 12(5), pp. 323–331. doi: 10.1002/1616-3028.
- [97] Meng, X., Liu, J., Jiang, Y., Chen, W., Lee, C., Bello, I. and Lee, S. (2003) 'Structure- and Size-Controlled Ultrafine ZnS Nanowires', *Chem. Phys. Lett.*, 382(3-4), pp. 434–438. doi: 10.1016/j.cplett.2003.10.093.
- [98] Cong, Q., He, X., Gao, M., Ma, X. and Li, G. (2014) 'ZnO/CuS Heterostructured Nanocomposite and Its Organic Functionalisation', *Mater. Res. Innov.*, 18(4), pp. 740–746. doi:10.1179/1432891714Z.
- [99] Yu, X. and An, X. (2010) 'Controllable Hydrothermal Synthesis of Cu₂S Nanowires on the Copper Substrate', *Mat. Lett.*, 64(3), pp. 252–254. doi:10.1016/j.matlet.2009.10.051.
- [100] Hsu, C.L., Tsai, J.Y. and Hsueh, T.J. (2015) 'Novel field emission structure of CuO/Cu₂O composite nanowires based on copper through silicon via technology', *RSC Adv.*, 5(43), pp. 33762–33766. doi: 10.1039/c5ra03513a.
- [101] Kar, S. and Chaudhuri, S. (2004) 'Solvothermal synthesis of nanocrystalline FeS₂ with different morphologies', *Chem. Phys. Lett.*, 2004, 398(1-3), pp. 22–26. doi:10.1016/j.cplett.2004.09.028.
- [102] Whittaker-Brooks, L., Gao, J., Hailey, A., Thomas, C., Yao, N. and Loo, Y.L. (2015) 'Bi₂S₃ nanowire networks as electron acceptor layers in solution-processed hybrid solar cells', *J. Mater. Chem. C*, 3(11), pp. 2686–2692. doi: 10.1039/c4tc02534b.
- [103] Mangham, S. C., Alam Khan, M., Benamara, M. and Manasreh, M. O. (2013) 'Synthesis of iron pyrite nanocrystals utilizing trioctylphosphine oxide (TOPO) for

photovoltaic devices’, *Materials Letters*. Elsevier, 97, pp. 144–147. doi: 10.1016/j.matlet.2013.01.101.

[104] Murphy, R. and Strongin, D. R. (2009) ‘Surface reactivity of pyrite and related sulfides’, *Surface Science Reports*. Elsevier B.V., 64(1), pp. 1–45. doi: 10.1016/j.surfrep.2008.09.002.

[105] Nikolić, M. V., Vujatović, S. S., Ivetić, T., Paraskevopoulos, K. M., Zorba, T. T., Aleksić, O. S., Blagojević, V., Nikolić, N. and Nikolić, P. M. (2010) ‘Optical far infrared properties of FeS₂’, *Optoelectronics and Advanced Materials, Rapid Communications*, 4(12), pp. 2000–2002.

[106] Lin, Y.Y., Wang, D.Y., Yen, H.C., Chen, H.L., Chen, C.C., Chen, C.M., Tang, C.Y. and Chen, C.W. (2009) ‘Extended red light harvesting in a poly(3-hexylthiophene)/iron disulfide nanocrystal hybrid solar cell.’, *Nanotechnology*, 20(40), p. 405207. doi: 10.1088/0957-4484/20/40/405207.

[107] Steinhagen, C., Harvey, T. B., Stolle, C. J., Harris, J. and Korgel, B. A. (2012) ‘Pyrite nanocrystal solar cells: Promising, or fool’s gold?’, *Journal of Physical Chemistry Letters*, 3(17), pp. 2352–2356. doi: 10.1021/jz301023c.

[108] Kirkeminde, A., Scott, R. and Ren, S. (2012) ‘All inorganic iron pyrite nano-heterojunction solar cells’, *Nanoscale*, pp. 7649–7654. doi: 10.1039/c2nr32097e.

[109] Richardson, B. J., Zhu, L. and Yu, Q. (2013) ‘Inverted hybrid solar cells based on pyrite FeS₂ nanocrystals in P3HT:PCBM with enhanced photocurrent and air-stability’, *Solar Energy Materials and Solar Cells*. Elsevier, 116, pp. 252–261. doi: 10.1016/j.solmat.2013.05.014.

- [110] Alam Khan, M., Sarker, J. C., Lee, S., Mangham, S. C. and Manasreh, M. O. (2014) ‘Synthesis, characterization and processing of cubic iron pyrite nanocrystals in a photovoltaic cell’, *Materials Chemistry and Physics*. Elsevier B.V, 148(3), pp. 1022–1028. doi: 10.1016/j.matchemphys.2014.09.013.
- [111] Bhandari, K. P., Koirala, P., Paudel, N. R., Khanal, R. R., Phillips, A. B., Yan, Y., Collins, R. W., Heben, M. J. and Ellingson, R. J. (2015) ‘Iron pyrite nanocrystal film serves as a copper-free back contact for polycrystalline CdTe thin film solar cells’, *Solar Energy Materials and Solar Cells*. Elsevier, 140, pp. 108–114. doi: 10.1016/j.solmat.2015.03.032.
- [112] Xuefeng, Q., Yi, X. and Yitai, Q. (2001) ‘Solventothermal Synthesis and Morphological Control of Nanocrystalline FeS₂’, *Mater. Lett.*, 48(2), pp. 109–111. doi: 10.1016/S0167-577X(00)00288-3.
- [113] Kar, S. and Chaudhuri, S. (2005) ‘Synthesis of Highly Oriented Iron Sulfide Nanowires through Solvothermal Process’, *Mater. Lett.*, 59(2-3), pp. 289–292. doi:10.1016/j.matlet.2004.10.005.
- [114] Li, L., Cabán-Acevedo, M., Girard, S. and Jin, S. (2014) ‘High-Purity Iron Pyrite (FeS₂) Nanowires as High-Capacity Nanostructured Cathodes for Lithium-Ion Batteries’, *Nanoscale*, 6(4), pp. 2112–2118. doi: 10.1039/c3nr05851d.
- [115] Yu, J., Wang, F., Wang, Y., Gao, H., Li, J. and Wu, K. (2010) ‘Interfacial Reaction Growth Approach to Preparing Patterned Nanomaterials and beyond’, *Chem. Soc. Rev.*, 39(5), pp. 1513–1525. doi: 10.1039/b812787p.

- [116] Patete, J., Peng, X., Koenigsmann, C., Xu, Y., Karn, B. and Wong, S. (2011) ‘Viable Methodologies for the Synthesis of High-Quality Nanostructures’, *Green Chem.*, 13(3), pp. 482–519. doi: 10.1039/c0gc00516a.
- [117] Li, Y., Han, Z., Jiang, L., Su, Z., Liu, F., Lai, Y. and Liu, Y. (2014) ‘Template-directed synthesis of ordered iron pyrite (FeS₂) nanowires and nanotubes arrays’, *J. Sol-Gel Sci. Technol.*, 72(1), pp. 100–105. doi: 10.1007/s10971-014-3425-2.
- [118] Kashiwaba, Y., Katahira, F., Haga, K., Sekiguchi, T. and Watanabe, H. (2000) ‘Hetero-epitaxial growth of ZnO thin films by atmospheric pressure CVD method’, *J. Cryst. Growth.*, 221(1-4), pp. 431–434. doi: 10.1016/S0022-0248(00)00729-6.
- [119] Bu, I. and Yeh, Y.M. (2012) ‘Effects of sulfidation on the optoelectronic properties of hydrothermally synthesized ZnO nanowires’, *Ceram. Int.*, 38(5), pp. 3869–3873. doi: 10.1016/j.ceramint.2012.01.038.
- [120] Öztürk, S., Kılınc, N., Taşaltın, N. and Öztürk, Z. (2012) ‘Fabrication of ZnO Nanowires and Nanorods’, *Physica. E*, 44(6), pp. 1062–1065. doi: 10.1016/j.physe.2011.01.015.
- [121] Lifson, M., Levey, C. and Gibson, U. (2013) ‘Diameter and Location Control of ZnO Nanowires Using Electrodeposition and Sodium Citrate’, *Appl. Phys. A*, 113(6), pp. 243–247. doi: 10.1007/s00339-012-7538-6.
- [122] Brayek, A., Ghoul, M., Souissi, A., Assaker, I., Lecoq, H., Nowak, S., Chaguetmi, S., Ammar, S., Oueslati, M. and Chtourou, R. (2014) ‘Structural and optical properties of ZnS/ZnO core/shell nanowires grown on ITO glass’, *Mater.Lett.*, 129(1), pp. 142–145. doi: 10.1016/j.matlet.2014.04.192.

- [123] Wu, D., Fan, X., Tian, K., Dai, J. and Liu, H. (2012) 'Fabrication and Photocatalytic Properties of Cu₂S/T-ZnO Heterostructures via Simple Polyol', **Process. Trans. Nonferrous Met. Soc. China**, 22(7), pp. 1620–1628. doi: 10.1016/S1003-6326(11)61365-4.
- [124] Zhao, X., Wang, P. and Li, B. (2010) 'CuO/ZnO Core/shell Heterostructure Nanowire Arrays: Synthesis, Optical Property, and Energy Application', **Chem. Commun.**, 46(36), pp. 6768–6770. doi: 10.1039/c0cc01610a.
- [125] Patra, A., Bendikov, M. and Chand, S. (2014) 'Poly(3,4-ethylenedioxy selenophene) and its derivatives: Novel organic electronic materials', **Acc. Chem. Res.**, 47(5), pp. 1465–1474. doi: 10.1021/ar4002284.
- [126] Rhoden, C. R. B. and Zeni, G. (2011) 'New development of synthesis and reactivity of seleno- and tellurophenes.', **Org. Biomol. Chem.**, 9(1), pp. 1301–1313. doi: 10.1039/c0ob00557f.
- [127] Liu, X., Wang, J., Zhang, J. and Yang, S. (2006) 'Sol-gel-template synthesis of ZnO nanotubes and its coaxial nanocomposites of LiMn₂O₄/ZnO', **Materials Science and Engineering A**, 430(1–2), pp. 248–253. doi: 10.1016/j.msea.2006.05.059.
- [128] Rätty, J., Peiponen, K.-E. and Asakura, Y. (2004) Definitions of Optical Instrumentation and Measurement. In: Rätty, J., Peiponen, K.-E. and Asakura, Y. **UV-Visible Reflection Spectroscopy of Liquids**. Berlin, Springer-Verlag Heidelberg, p. 85-95.
- [129] Rätty, J., Peiponen, K.-E. and Asakura, Y. (2004) Exploring the Insides of a Spectrophotometer. In: Rätty, J., Peiponen, K.-E. and Asakura, Y. **UV-Visible Reflection Spectroscopy of Liquids**. Berlin, Springer-Verlag Heidelberg, p. 99-139.

[130] Behzadi, S., Ghasemi, F., Ghalkhani, M., Ashkarran, A. A., Akbari, S. M., Pakpour, S., Hormozi-Nezhad, M. R., Jamshidi, Z., Mirsadeghi, S., Dinarvand, R., Atyabi, F. and Mahmoudi, M. (2015) ‘Determination of nanoparticles using UV-Vis spectra’, *Nanoscale*, pp. 5134–5139. doi: 10.1039/C4NR00580E.

[131] Shinde, K. N., Dhoble, S. J., Swart, H. C. and Park, K. (2012) Basic Mechanisms of Photoluminescence. In: Shinde, K. N., Dhoble, S. J., Swart, H. C. and Park, K. *Phosphate Phosphors for Solid-State Lighting*. Berlin, Springer-Verlag Heidelberg, pp. 41–60.

[132] Perkin Elmer (2000) Instrumentation. In: Perkin Elmer. *An Introduction to Fluorescence Spectroscopy*. London, Perkin Elmer Inc., p. 21-26.

[133] O’ Connor, T. and Zamkov, M. (2013) Optical Properties of Nanocomposites. In: Kumar, C. S.S.R. *UV-VIS and Photoluminescence Spectroscopy for Nanomaterials Characterization*. Berlin, Springer-Verlag Heidelberg, p. 485-530.

[134] Stuart, B. (2004) Spectral Analysis. In: Stuart, B. *Infrared Spectroscopy: Fundamentals and Applications*. U.S.A., Wiley, p. 45-70.

[135] Stuart, B. (2004) Experimental Methods. In: Stuart, B. *Infrared Spectroscopy: Fundamentals and Applications*. U.S.A., Wiley, p. 15-44.

[136] Lee, M. (2016) PART I: X-RAYS AND CRYSTAL GEOMETRY. In: Lee, M. *X-Ray Diffraction For Materials Research. From Fundamentals to Applications*. U.S.A., CRC Press, p. 4-25.

[137] Leng, Y. (2008) X-ray Diffraction Methods. In: Leng, Y. *Materials Characterization. Introduction to Microscopic and Spectroscopic Methods*. Singapore, Wiley, p. 45-78.

- [138] Lee, M. (2016) DIRECTIONS OF X-RAY DIFFRACTION. In: Lee, M. *X-Ray Diffraction For Materials Research. From Fundamentals to Applications*. U.S.A., CRC Press, p. 117-180.
- [139] Egerton, R. F. (2005) The Scanning Electron Microscope. In: Egerton, R. F. *Physical principles of electron microscopy: An introduction to TEM, SEM, and AEM*, U.S.A., Springer, p. 125-154.
- [140] Lupini, A.R., Rashkeev, S. N., Varela, M., Borisevich, A. Y., Oxley, M. P., *et al.* (2015) Scanning Transmission Electron Microscopy. In: Kirkland, A. I. and Haigh, S. J. *Nanocharacterisation*, London, RSC, p. 30-74.
- [141] Inada, H. and Zhu, Y. (2015) Secondary Electron Microscopy in STEM. In: Tanaka, N. *Scanning Transmission Electron Microscopy of Nanomaterials: Basics of imaging and analysis*, London, Imperial College Press, p. 307-341.
- [142] Fultz, B. and Howe, J. (2013) The TEM and Its Optic. In: Fultz, B. and Howe, J. *Transmission Electron Microscopy and Diffractometry of Materials*, Berlin Springer-Verlag Heidelberg, p. 59-109.
- [143] Smith, D.J. (2015) Characterization of Nanomaterials Using Transmission Electron Microscopy. In: Kirkland, A. I. and Haigh, S. J. *Nanocharacterisation*, London, RSC, p. 1-26.
- [144] Williams, D. and Carter, B. (2009) The Transmission Electron Microscope, In: Williams, D. and Carter, B. *Transmission Electron Microscopy. A Textbook for Materials Science*, Berlin Springer-Verlag Heidelberg, p. 3-17.
- [145] Kissinger, P. T. and Heineman, W. R. (1983) ‘Cyclic voltammetry’, *Journal of Chemical Education*, 60(9), pp. 9242–5. doi: 10.1002/anie.201004874.

- [146] Bard, A.J. and Faulkner, L.R. (2000) Basic Potential Step Methods. In: Bard, A.J. and Faulkner, L.R. *Electrochemical Methods. Fundamentals and Applications*, U.S.A., Wiley, p. 226-260.
- [147] Bard, A.J. and Faulkner, L.R. (2000) Techniques Based on Concepts of Impedance. In: Bard, A.J. and Faulkner, L.R. *Electrochemical Methods. Fundamentals and Applications*, U.S.A., Wiley, p. 226-260.
- [148] Rusling, J. F. and Suib, S. L. (1994) ‘Characterizing Materials with Cyclic Voltammetry’, *Advanced Materials*, 6(12), pp. 922–930. doi: 10.1002/adma.19940061204.
- [149] Monk, P. (2001) Additional Methods. In: Monk, P. *Fundamentals of Electro-Analytical Chemistry*, U.S.A., Wiley, p. 237-274.
- [150] Orazem, M. E. and Tribollet, B. (2008) Electrochemical Instrumentation. In: Orazem, M. E. and Tribollet, B. *Electrochemical Impedance Spectroscopy, Analysis*. U.S.A., Wiley, p. 97-105.
- [151] Macdonald, J.R. and Johnson, W.B. (2005) Fundamentals of Impedance Spectroscopy. In: Barsoukov, E. and Macdonald, J. R. *Impedance Spectroscopy: Theory, Experiment, and Applications*, U.S.A., Wiley, p. 1-26.
- [152] Loveday, D., Peterson, P. and Rodgers, B. (2004) ‘Evaluation of Organic Coatings with Electrochemical Impedance Spectroscopy Part 1: Fundamentals of Electrochemical Impedance Spectroscopy’, *JCT coatings tech*, 1(1), pp. 46–52.
- [153] Brown, M. E. (2009) Introduction. In: Brown, M. E. *Introduction to Thermal Analysis Techniques and Applications*. U.S.A., Kluwer Academic Publishers, p.1-11.
- [154] Brown, M. E. (2009) Thermogravimetry (TG). In: Brown, M. E. *Introduction to*

Thermal Analysis Techniques and applications. U.S.A., Kluwer Academic Publishers, p.19-52.

[155] Brown, M. E. (2009) **Differential Thermal Analysis (DTA) and Differential Scanning Calorimetry (DSC)**. In: Brown, M. E. *Introduction to Thermal Analysis Techniques and applications*. U.S.A., Kluwer Academic Publishers, p.55-89.

[156] W. Hemminger W. and Sarge, S.M. (2003) Thermal Analysis and Calorimetry-Definitions, Classifications and Nomenclature. In: Patrick K. Gallagher. *Handbook of Thermal Analysis and Calorimetry. Principles and Practice*, U.S.A., Elsevier, p. 7-30.

[157] Gabbott, P. (2007) A Practical Introduction to Differential Scanning Calorimetry. In: Gabbott, P. *Principles and Applications of Thermal Analysis*, U.S.A., Blackwell publishing, p. 1-51.

[158] Höhne, G.W., Hemminger, W. and Flammersheim. (1996) Types of Differential Scanning Calorimeters. In: Höhne, G.W., Hemminger, W. and Flammersheim. *Differential Scanning Calorimetry An Introduction for Practitioners*, Berlin, Springer-Verlag Heidelberg , p. 7-14.

[159] Höhne, G.W., Hemminger, W. and Flammersheim. (1996) Applications of Differential Scanning Calorimetry. In: Höhne, G.W., Hemminger, W. and Flammersheim. *Differential Scanning Calorimetry An Introduction for Practitioners*, Berlin, Springer-Verlag Heidelberg , p. 105-180.